Journal of Inorganic and Organometallic Polymers and Materials (2022) 32:741–772
https://doi.org/10.1007/s10904-021-02198-5

TOPICAL REVIEWS

Room-Temperature Chemiresistive Gas Sensing of SnO_2 Nanowires: A Review

Vraj Shah[1] · Jaydip Bhaliya[1] · Gautam M. Patel[2] · Priyanka Joshi[3]

Received: 13 November 2021 / Accepted: 10 December 2021 / Published online: 22 January 2022
© The Author(s), under exclusive licence to Springer Science+Business Media, LLC, part of Springer Nature 2021

Abstract

Innovative chemiresitive gas sensors with strong sensing qualities that operate at room temperature are much more appealing due to their properties of long-life cycle, high stability, and lower usage of power. As we know, n-type semiconducting metal oxide like SnO_2 received a lot of interest for its gas sensing applications. The rapid progress of different synthesis processes has allowed researchers to investigate a wide range of new nanostructures and their incorporation into smart gas sensing devices. Generally, conventional metal oxide-based sensors are functioned at very high a temperature, which causes high power consumption and low selectivity. Therefore, to remove this issue, metal oxides doped with various nanostructures are the first choice due to their advantages: high surface-area-to-volume ratio, efficient electron transfer, improved and adjustable surface reactivity, and quick access response time, and short recovery time. In this review, we have discussed the preparation of SnO_2 nanowires through various methods and discussed the state of the art of vapour or gas sensors based on tin oxide nanowires and can exhibit sensing properties at room temperature. An overview of the wealth of material, methods, and sensing mechanisms like response time, analytical ranges, and operating temperatures are also explained. In the last section, we discussed the current status and challenges and depicted the potential future aspects.

Keywords SnO_2 nanowires · Semiconductor material · Gas sensing · Room temperature operation

1 Introduction

In recent times, toxic and hazardous gases produced as waste from various industries and household activities cause air pollution in the environment, even if the government in each nation has set a particular limit that if the concentration of the gas exceeds the limit, pollution occurs [1–4]. As industrialization and urbanization expand, various volatile organic compounds (VOCs) and hazardous gases are released into the environment, inflicting alarming damage and jeopardising human society's sustainability [5–7].There has been a substantial increase in global concern about environmental pollution, prompting society to seek out gas detection devices for monitoring and measuring these hazardous and life-threatening noxious chemical gases. Therefore, Gas detectors are commonly utilised in a variety of applications, comprising industries, cars, mining, and environmental monitoring, both outdoors and indoors [8, 9]. Apart from this, these gases are present at low levels in the atmosphere, in the parts per billion (ppb) ranges. This is because the surface-gas contact is poor, just little chemisorption, mostly physisorption, occurs, making electronic detection nearly difficult. As a result, developing a gas sensor that is both sensitive and effective is necessary to identify hazardous gases [10]. Moreover, the gas sensing industry is presently worth €630 million per year, with chemiresistive sensors accounting for €230 million due to its inexpensive price, excellent sensitivity, rapid reaction, and relative ease [11–13].A gas sensor is a device that transforms the concentration of gas into electrical impulses [14]. Gas sensors are available in a number of configurations, including electrochemical gas sensors, metal oxide semiconductor (MOS) gas sensors, and infrared gas sensors. [15–25].Gas sensors made of metal oxide semiconductors, in particular, have swiftly

✉ Gautam M. Patel
gautampatel1573@yahoo.co.in

[1] Department of Chemistry, School of Science, ITM SLS Baroda University, Vadodara, GJ 391510, India

[2] Department of Industrial Chemistry, Institute of Science & Technology for Advanced Studies & Research (ISTAR), CVM University, V.V. Nagar, Anand, GJ 388120, India

[3] São Carlos Institute of Physics, University of São Paulo, Box 369, São Carlos, SP 13566-970, Brazil

turned into a hotspot in contemporary gas sensor research due to benefits for example low cost, high reaction speed, easy development, and extended service life [26–28].The sensor-based on MOS can be classified into two categories; resistive and non-resistive gas senor and SnO_2 based gas sensor fall into the category of a resistive type that follows the surface-controlled model. The in-depth mechanism for this has been discussed below [29].

Furthermore, conventional metal oxide gas sensors (WO_3-SnO_2, ZnO-SnO_2, CdO-MnO_2, TiO_2-V_2O_5, and ZnO-CdO) [1] have several drawbacks like, they usually operate at a very high temperature which varies from 100 to 400 °C, which causes the high-power consumption, as well as the stability and life span of the sensor, would be decreased [30–33]. Henceforth, the demand for the synthesis metal oxide semiconductor (MOS) sensor and application to sense gas at room temperature has been increased drastically, and that is possible with the metal oxide combination with zero-dimension, one dimension (nanowires, nanorods, and nanobelts) two dimension, and three dimensions nanostructures. These kinds of sensors lead to high sensitivity, quick response time, easy recovery, low maintenance excreta [34–42]. Out of other nanostructures, nanowires, structures having constrained to tens of nanometer or less and an unconstrained longitudinal size, they exhibit aspect ratio (length-to-width ratio) of 1000 or more, they are one-dimensional (1-D) material also nanowires shows quantum mechanism so that they called quantum nanowires. When this type of nanomaterial is incorporated with semiconducting material like SnO_2 can exhibit the property required for an ideal sensor that operates at room temperature, like excellent sensitivity, superior reproducibility, fast reaction and recovery time, and to a name of a few [43–46].

1.1 General Properties and Structure of Tin Oxide (SnO_2)

Tin oxide is the n-type semiconductor material with a bandgap of (Eg = 3.6 eV at 300 K), that creates transparent conducting electrodes for solar cells, organic light-emitting diodes, and gas sensors [47]. In addition to that, the properties of SnO_2 have been depicted in Table 1 [48]. SnO_2 comprises orthomorphic and tetrode systems, the crystal structure of it may alter as a result of pressure. The sequence of transformations is rutile-type ($P4_2/mnm$) → $CaCl_2$-type (Pnnm) α-PbO_2 type (Pbcn) → pyrite-type (Pa^3(—))ZrO_2-type (Pbca), (As shown in Fig. 1). It converts into fluorite (Fm^3 (—) m) as well as cotunnite-type at greater pressures and temperatures (Pnam).The rutile structure with a tetragonal shape is the most popular and frequently used SnO_2 sensor at room temperature. The SnO_2 cell, Sn^{4+} fills the tetrahedron's top and centre, while O_2 lodges certain places within the tetragonal rutile structure. There are two Sn atoms and four O atoms in each SnO_2 crystal cell. Formation of a 90-degree angle between three crystal axes occurs with each other, that is, α = β = γ = 90° with lattice parameters of a = b = 4.737 Å, c = 3.186 Å [49–52]. Here, types of oxidation state tin carry + 2 and + 4; thus, two types of oxides can be created, such as stannous oxide (SnO) and stannic oxide (SnO_2); from these two oxides SnO_2 is very stable [53–57].

Table 1 Properties of tin oxide (SnO_2) [48]

Chemical name	Tin oxide (SnO_2) Stannic oxide
Crystalline system	Tetragonal
Space group	$P4_2/mnm$
Cell parameter (Å)	4.738 × 4.738 × 3.187
"a" × "b" × "c"	< 90° × 90° × 90° >
Density	6.99 g/cm^3
Melting point	1898 K
Hardness	6–7 Mohs
Colour	Transparent (single crystal) or white (polycrystalline)
Optical bandgap	3.4–3.7 eV
Fundamental bandgap	3.4–3.7 eV
Position of VBM (ionization energy)	~ − 9 eV
Electrical classification	n-Type semiconductor
Dielectric constant	9.0

1.2 Properties of SnO_2 Nanowire for Gas Sensing

As the basic physical properties of tin oxide is discussed above. However, to understand the compatibility property of the SnO_2 in the nanoscale material let's take the view from historical background to the state -of- the art of the material. The first nanostructure which consists of the SnO_2 had been developed in the year 1984 by Nagano et al. [54]. Apart from this, expression of significant property of the tin is because of the dual vacancy in the Sn by means of depending on the oxygen chemical potential of the system, the dual valency permits a reversible shift of the surface composition from stoichiometric surfaces with Sn^{4+} surface cations to a reduced surface with Sn^{2+} surface cations. Surface reduction alters the electrical structure of the surface by forming Sn5s derived surface states deep within the band gap, as well as decreasing the working temperature [55]. This property leads the material would have the large number of atoms on the surface, and the effective van der Waals, Columbic and interatomic coupling occur [49]. As a result, low-dimensional oxide materials such as nanoparticles, nanospheres, nanorods, nanowires, nanoribbon/nanobelts, nanotubes, nanodisks, and nanosheets elicit a wide range of interest for the applications in various fields including gas sensor. Henceforth, with the goal of acquiring improved

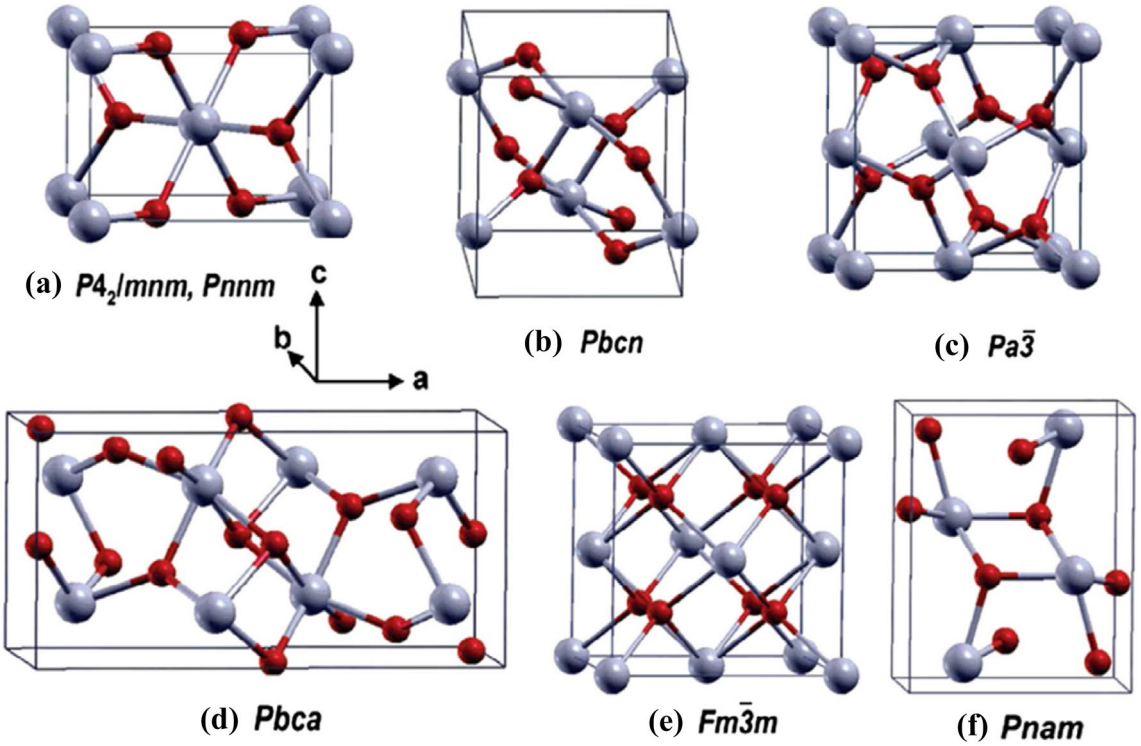

Fig. 1 SnO_2 polymorph crystal formations. **a** Rutile ($P4_2/mnm$) and $CaCl_2$ type (Pnnm), **b** a-PbO_2-type (Pbcn), (**c**) pyrite (Pa_3—), **d** ZrO_2-type (Pbca), **e** fluorite (Fm^3—m), and **f** cotunnite (Pnam) [10]

and tailored properties, there has been a growing trend to synthesise novel forms of SnO_2 ranging from thick and thin films to nano-scale objects such as nanowires, nanofibers, nanopowder, and nanorods. The most desirable properties that may be obtained utilising nanowires in the field of gas sensors are enhanced sensitivity, selectivity, and thermal stability, as well as speed of response and recovery. This is due to the high crystallinity, production of fewer agglomerated structures, and the huge surface-to-volume ratio. The atoms positioned just at the surface, where the sensor transduction process takes place, play a critical role (domination) in such structures, resulting in improved chemical sensing performance (such as catalytic activity or surface adsorption) [56].

Furthermore, let's see the mechanistic view for the question, why? Nanowire is only used for gas sensing and how it feasible in comparison with other nanostructures with main SnO_2. Since, this review article depicts the sensing operating temperature of RT, so high temperature operation has been eliminated. As we all know, the gas sensing phenomena is based on electron transfer between the Sensing material and the target gases, with the depletion layer forming or deforming depending on the kind of material. The passivation of dangling bonds or incomplete covalent bonds, or the accessible rapid surface states generated by the huge surface: volume ratio in nanowire systems, may be responsible for RT sensing. Because of the arbitrary oxygen concentration, the target gases are likely to make transient bonds with nanowire surface vacancies. These bonds serve as electron-transfer bridges between the gas and the nanowire surface. This is owing to the unstable oxygen content in oxide materials, however it is worth mentioning that controlling the oxygen concentration in any oxide material is challenging. Under some conditions, the gas molecules can be broken down into their atomic components due to the extremely high reactivity of incomplete bonds or rapid surface states. Chemisorption is the consequence of the suggested passivation process of the bonds induced by unstable oxygen. Because of the length difference, controlling the oxygen level throughout a nanoparticle is easier than controlling it throughout a nanowire. As a result, bond passivation in nanowire formations is more common than in nanoparticles. The charge carriers responsible for gas sensing proceed in a straight path if the sensing materials are in nanowire form. This reduces carrier dispersion during conduction and increases the material's gas sensitivity. Furthermore, because nanowire is a single crystalline structure with set growth orientations, it reduces instabilities caused by percolation and hopping, boosting overall material stability. Specific effects like as self-heating can only be achieved by building nanowire-based devices. Indeed, the current flowing through a device composed of a single nanowire connected by two electrodes, which functions as a sensor signal, is enough to warm the nanowire by

Joule effect up to the temperature required to activate the gas sensing reactions, and the selectivity of the sensor will be increased due to the fast reaction [57].

1.3 Metal Oxide as Gas Sensors

The sensor performances of the sensor based on MOS are strongly reliant on the temperature, which affects the kinetics of the process and the conductivity and electron mobility [58–60]. Usually, there is a need to provide temperature on the sensor's surface to cross the activation energy barrier, which subsequently enhances the kinetics sensing detection [13, 27, 28, 61]. On the other hand, the high-temperature operation restricts its extensive applicability since it represents energy waste, which goes counter to our society's advocacy for energy conservation and emission reduction. Furthermore, the high-temperature operation produces sensor instability, which might result in inaccurate or erroneous test findings. As a result, the essential goal is to reduce the working temperature of MOS-based gas sensors [62–64]. The MOS-based sensor that operates at room temperature does not require a heater, which is possible using the current evolving trend, so this would provide a cheaper and energy-saving feature of the sensor. The room-temperature operation significantly allowed for reduced energy consumption and the danger of a gas explosion (some gas ignited at a specific temperature in the atmosphere) and improved long-term stability, which is a developing issue [65–68].On the contrary, due to the low thermal energy, a small number of thermal electrons may be located on the MOS surface while the sensor is run at ambient temperature, resulting in the formation of a few oxygen species. Because of the high adsorption energy, this tiny group of oxygen species is thermally stable and difficult to remove from the surface resulting in poor sensing characteristics [69–71]. Aside from them, relative humidity (RH) is a major source of interference in the room-temperature performance of MOS-based gas sensors [72–74]. In a moist environment, H_2O molecules compete with oxygen molecules for surface reaction sites, restricting oxygen adsorption. The quantity of oxygen species drops as RH surges, resulting in a drop-in baseline resistance in the ambient environment and reduced sensor response [61, 75, 76].The MOS-based sensor that works at room temperature is studied chiefly under dry air conditions and various RH conditions. In summary, the greatest difficulty we have is lowering the working temperature of MOS sensors.

Here, the focus has been devoted to Tin oxide nanowires for the sensing applications at room temperature because of the various advantages like the way of electron transfer (length of NWs), increased as well as surface reactivity is controllable, meaning that room-temperature functioning is conceivable, quicker recovery along with response time, dimensions can be compared to the allowance of the surface charge region, large scale production can be done by relatively simple preparation methods, affordable to use, fabrication, as well as manipulation, is very easy, high integration density, lesser consumption of electricity and smaller size, these are the merits of metal oxide nanowires sensors. Now, specifically, tin oxide-based nanowires merits are utilized widely for optoelectronic devices and gas sensors which can measure leakages of reducing gases and oxidizing because of its high surface to volume ratio and so on [77, 78].Till today, several articles in review on sensing methods or target gases have concentrated on the design and development of novel tin oxide nanomaterials. For instance, Meng et al. had explained the brief review on metal oxide nanostructures for detecting gases but mainly focused on morphology and the operating temperature mentioned in it above the RT [16]. Then, Li et al. had published a review that focused on composite base tin oxide nanomaterial as chemiresistive gas sensor, however, nowhere mentioned the application of sensing gases at RT, and all types of nanomaterials have been explained in combination with tin [79]. Besides this, Wang et al. had reported the review based on tin oxide nanostructures that detect hazardous and toxic gases. Still, they nowhere described the morphology of tin oxide nanowire with an application of sensing at RT [10].

On the other hand, as far as we know, no brief review report on SnO_2-based nanowires for gas detection applications at room temperature has been published. So, our aim here is a thorough overview of current advancements in SnO_2 NWs, with expectations for future works toward creating higher performance gas sensors. This comprehensive review elicits the SnO_2nanowires with cutting-edge design and precise gas-sensing characteristics. The first section covers the sensing mechanism of chemiresistive gas sensors, and then the second part consists of different synthesis approaches of the SnO_2 NWs. Here, Fig. 2a illustrates the general overview of this review paper, which comprises the detection of various gases by SnO_2 NWs, its fabrication methods, and morphology. Then, Fig. 2b shows the graphical representation of publications regarding tin oxide nanowires from the past ten years.

1.4 General Gas Sensing Mechanism of Chemiresistive Gas Sensor

As we know that, chemiresistive gas sensors are dependent on a semiconducting material. Semiconducting materials are classified into two categories; n-type and p-type [80–84]. Here, SnO_2 nanowire falls under the category of n-type semiconducting material. First, to begin with, the mechanisms, oxygen molecules present in the fresh air are adsorbed on the surface of sensing material (SnO_2 NWs). Since the sensing material is n-type semiconducting, the electrons flow would

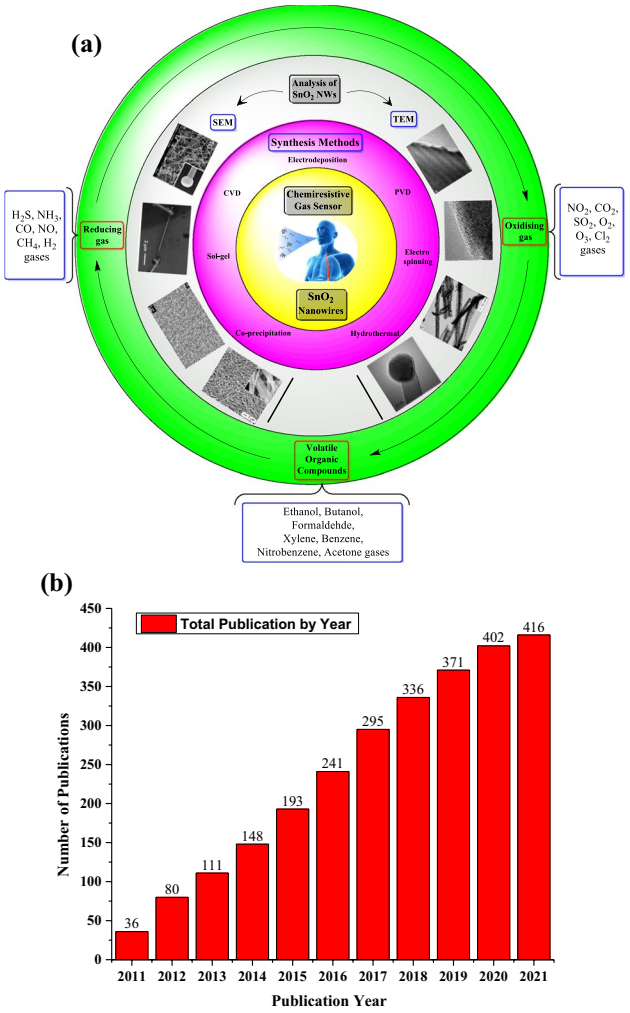

Fig. 2 **a** Schematic diagram of Tin oxide nanowires as a gas sensor for detecting toxic gases and volatile chemical compounds (VOCs), **b** the total number of articles published on tin oxide nanowire throughout the previous decade (PubMed, accessed on 20th July 2021, Keyword search: tin oxide + nanowires)

be there inside the sensing material (conduction band), due to the adsorption of oxygen occurring on the surface that removes the electrons which flow inside the sensing material and converts into the oxygen ions. Hence, the resistance of the SnO_2 will be increased. If the reducing gas is attributed to the oxygen ions, the stored electrons are released inside the conduction band of sensing material, which decreases the resistance. The change in resistance can be converted into an output signal known as the sensor's sensitivity. The same process occurs in the case of p-type semiconducting materials but in a reverse manner. When oxidizing gas approaches the surface of oxygen ions of the tin oxide, then resistance will be increased instead of decreased [85–89]. Table 2 and Fig. 3 below portrayed the sensing mechanism in p and n-type semiconducting materials [90]. Moreover,

Table 2 When MOS is exposed to specific oxidising and reducing gases, its resistance varies

Semiconductor	Reducing gas (CO, NH_3, H_2, etc.)	Oxidizing gas (NO_2, CO_2, etc.)
n-type	Resistance decrease	Resistance increase
p-type	Resistance increase	Resistance decrease

the mechanism of sensing in reducing gas approaching the surface of tin oxide has been illustrated in Fig. 4b [85, 91].

The resistance decreases when reducing gas adsorbed on the surface of oxygen ions that can be called the bend bending [86], and the graph between resistance versus time when the surface is exposed in the air and in the presence of reducing gas has been depicted in Fig. 4a [91, 92]. The generation of oxygen ions (O^{2-}, O_2^-, and O^-) strongly depends on the temperature. The reaction below shows the generation of oxygen ions with variation in the temperature [12].

O_2 molecules, for example, produce oxygen ion molecules at lower temperatures (room temperature to 150 °C), as specified by the Eq. (1):

$$O_{2(g)} + e^- \leftrightarrow O^-_{2(ads)} \tag{1}$$

The O_2 molecule dissociates in single or double oxygen ion atoms at a higher temperature, taking an electron from CB (conductance band). As specified by Eqs. 2 and 3:

$$1/2O_2 + e^- \leftrightarrow O^-_{(ads)} (150-300\,^{\circ}C) \tag{2}$$

$$1/2O_2 + 2e^- \leftrightarrow O^-_{2(ads)} (>300\,^{\circ}C) \tag{3}$$

When the adsorbed oxygen removes electrons, the layer generates a depletion layer or space charge layer (Δair). Apart from this, one more significant concept in the gas sensing mechanism is the Debye length (L_d), which states the depletion layer's depth, which concerns the distance amongst the surface of the metal oxide sensor and the point where the electrons are extracted [93]. The L_d of a gas detector is mainly determined through the operating temperature as well as charge carrier quantity [94], which may be stated as follows:

$$L_d = \sqrt{\frac{\varepsilon K_b T}{q^2 N_d}} \tag{4}$$

The material's dielectric constant, the Boltzmann constant, the operating temperature, electron charge, and charge carrier concentration are signified by b, T, q (1.6×10^{-19} C), and N_d, correspondingly [95].Besides this, the passage of streams of electrons from one grain to another is blocked because the polycrystalline sensing materials are linked

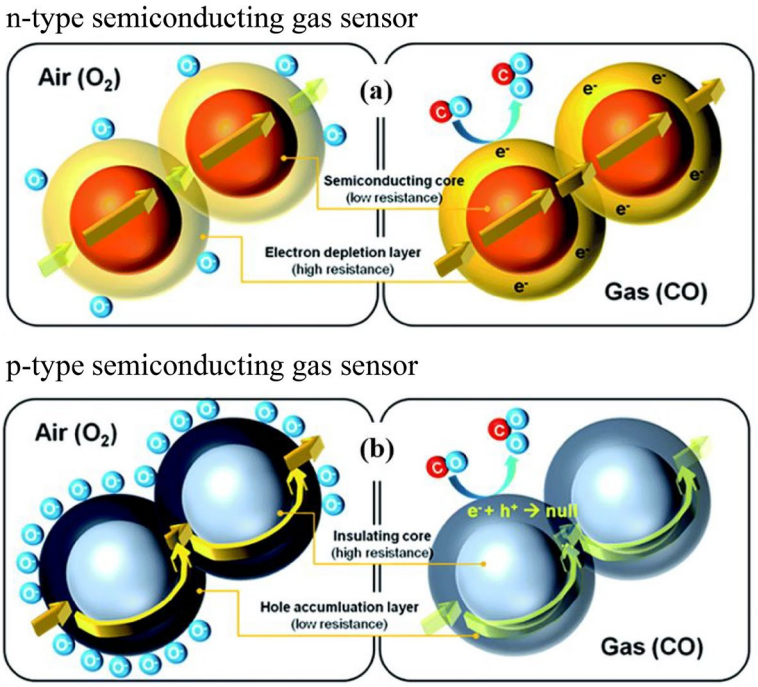

Fig. 3 Design of a semiconducting material-based sensing mechanism for n-type and p-type gas sensors [90]

with many grain boundaries. As illustrated in Fig. 4c, these results in the appearance of a potential barrier (V) on the surface. The sensor resistance increased as a result of polycrystalline sensing material. Then, the number of oxygen molecules adsorbed determines the height of potential berries [96, 97].

The adsorption process may be done in two ways; physisorption and chemisorption. Apart from this, three factors, namely the receptor and transducer functions, and the utility factor, influence the detecting property of a gas sensor [94, 98, 99]. The receptor function of a gas detector recognises molecules of oxygen and the gas to be detected in the surrounding environment via a sensing layer. Gas molecule adsorption is strongly dependent on the surface area of the sensing material. Changes in the form, morphology, and size of prepared materials, on the other hand, have the potential to alter the surface area. Aside from that, the transducer function is responsible for translating electrical changes affected by interactions between the sensor material and the gases being measured into a signal output in the form of resistance change. The utility factor facilitates the passage of gas molecules through the pores of sensing materials, which influences the response [2, 94]. Three of the variables described above can be utilised in the creation of novel materials for gas sensor applications. Other significant assessment criteria for the gas sensor function are reversibility, sensitivity, selectivity, stability, responsiveness, recovery time, and limit of detection (LOD). To begin, the term sensitivity (S) can be described as a shift in resistance (R) in response to a particular concentration of gas (C). If the target gas is reducing, it may be represented as Ra/Rg, whereas the oxidising gas can be stated as Rg/Ra. Ra denotes gas resistance in the fresh air, while Rg denotes goal gas resistance. Because of the differences in resistances, it may be written as [(Ra − Rg)/Ra]*100% [100, 101]. Second, response time may be defined as the difference between 90% sensor resistance increases in the presence of analyte gas and 90% resistance recovery following the withdrawal of a target gas, which is also known as recovery time [102]. Third, selectivity is an important chemiresitive sensor property. Cross-sensitivity happens when a gas-sensing device is susceptible to other interfering gases, such as test gas, causing a false alarm when detecting gas. Selectivity refers to a gas-sensing device's ability to identify a specific gas from other interfering gases [103, 104]. The selectivity of the sensor can be increased by (i) incorporating suitable additives, (ii) temperature control, (iii) using appropriate filters, (iv) UV-light illumination [104]. The capacity to detect the lowest possible concentration of an analyte using a sensor at a specific operating temperature is described as the LOD [105]. A chemiresitive sensor's stability is described as a gas sensor's capacity to give repeated data over a specific time period [32].

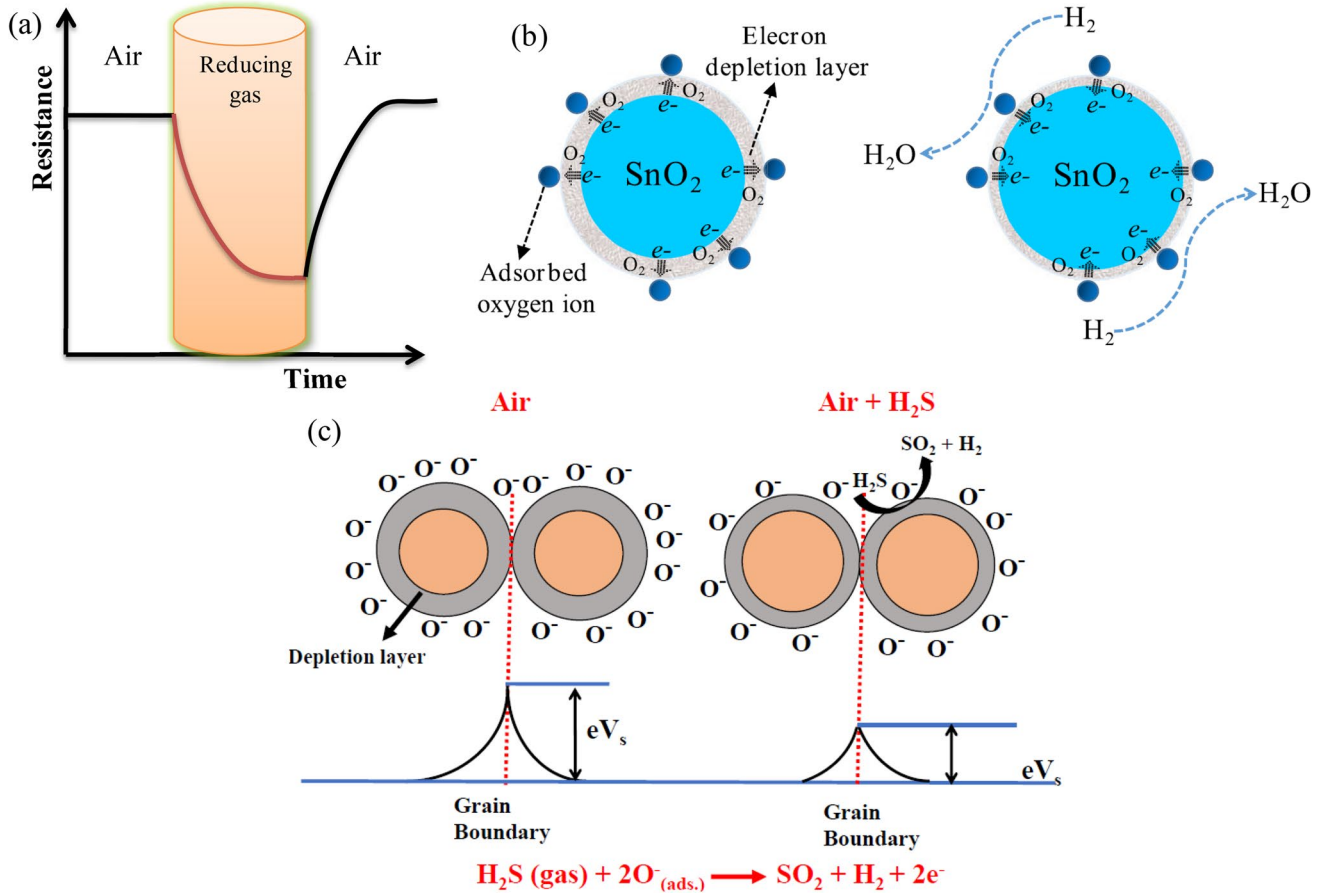

Fig. 4 **a** Resistance vs. time graph indicates the resistance change while exposed in air and reducing gas, **b** sensing mechanism of n-type semiconducting SnO_2 by the exposure of H_2 gas, and shows the change electrical moment in depletion layer as well as surface of the SnO_2, **c** Sensing mechanism of polycrystalline material; indicates the potential barrier (eV_s) change between grain boundaries in the exposure of air (left side) and the exposure of H_2S gas (right side) [85, 91]

2 Various Methods for the Synthesis of Tin Oxide Nanowires (SnO_2 NWs)

The gas detecting characteristics of SnO_2 gas sensors with various morphologies have been highly diverse; these qualities have piqued the scientific attention of many researchers. SnO_2 with different morphologies may be synthesized using a variety of preparation techniques. The gas detecting characteristics of the sensors are directly connected to the distribution and shape of SnO_2 products. As a result, techniques for preparing SnO_2 with varied morphologies have been devised to display specific characteristics and achieve desired outcomes [106]. However, in this communication, we have considered only one single morphology that is nanowire reinforced with SnO_2. There are four types of processing paths progressed for the development of SnO_2 nanowires: (I) wet processing, (II) molten processing, (III) solid processing, and (IV) vapour processing methods [107]. Despite this, the most common route for synthesizing tin oxide nanowire is wet processing, also known as the bottom-up approach. Figure 5 elicits the top-up and bottom-down approach for the synthesis of tin oxide nanowires [108]. The merits and demerits of each methods have been depicted in Table 3.

2.1 Co-precipitation Method

This method is straightforward to operate, cheaper, and does not need enormous pressure and temperature. Through changing the pH of the medium, starting material concentration and reagents for precipitating, particle size and shape can be controlled. By utilizing filtration and repeating washing, impurities in the precipitate can be easily removed. On the other hand, during the literature, it was found that particular nanowires are not manufactured by the co-precipitation method. Still, composites of tin oxide nanowires have been fabricated, and they also give gas sensing properties [109]. An example of SnO_2 NWs by co-precipitation method

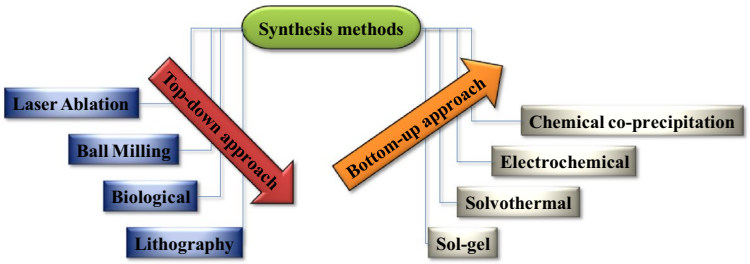

Fig. 5 Bottom-up and Top-down approach for the manufacture of tin oxide nanowires [108]

Table 3 Advantages and disadvantages of the methods used to synthesis SnO_2 nanowires

Method	Merits	Demerits	References
Hydrothermal	Simple to operate	Precise control over hydrothermal route still need to be addressed	[179]
	Not required costly equipment	Difficult to determine optimized parameters while preparing metal oxide nanostructures	
	High yield		
	Low energy consumption		
	Controlled morphology of nanostructures obtained		
	One-step fabrication process		
	Controlled size and shape of nanostructures obtained		
Co-precipitation	Controlled morphology nanostructure can be obtained	Calcination process and post-annealing process required	[180]
	No extensive equipment needed	Poor crystalline structure may obtained	
Sol–gel	Products have higher purity, are easy to prepare in different sizes	Organic solvents have a slower reaction time and are toxic to the human body	[120]
	A controllable degree of porosity		
	Nanowires are easy to prepare in different size		
Electrospinning	Low cost	Limited control pore structure	[181]
	Simple handling	Widely associated to produce polymeric nanofibers rather than, metal oxide nanowires	
	Minimal solution use		
	Easy and reproductive character		
	Obtained controlled diameter of nanowire		
Polyol	Stoichiometry control, size dimensions, size distribution, and so on	Low producibility	[129]
		Obtained Sensitive morphology	
CVD	Avoids the line-of-sight	High temperature operating condition	[182]
	High deposition rate	Possibility of toxicity of precursor	
	Production of thick coating layer	Mostly inorganic material are used	
	Highly porous nanostructures obtained		
PVD	Atomic level control of atomic composition	Line-on-sight deposition	[182]
	Not required the usage of special precursor	Low deposition rate	
	Safer then CVD due to absence of toxic precursors	Production of thin coating layer & annealing time required	
Electrodeposition	Rapid synthesis time	Nanomaterial with poor active sites formed	[184]
	Absence of chemical reductants and oxidants	Desired nanomaterial dimension cannot not received	
	No undesired product formed		

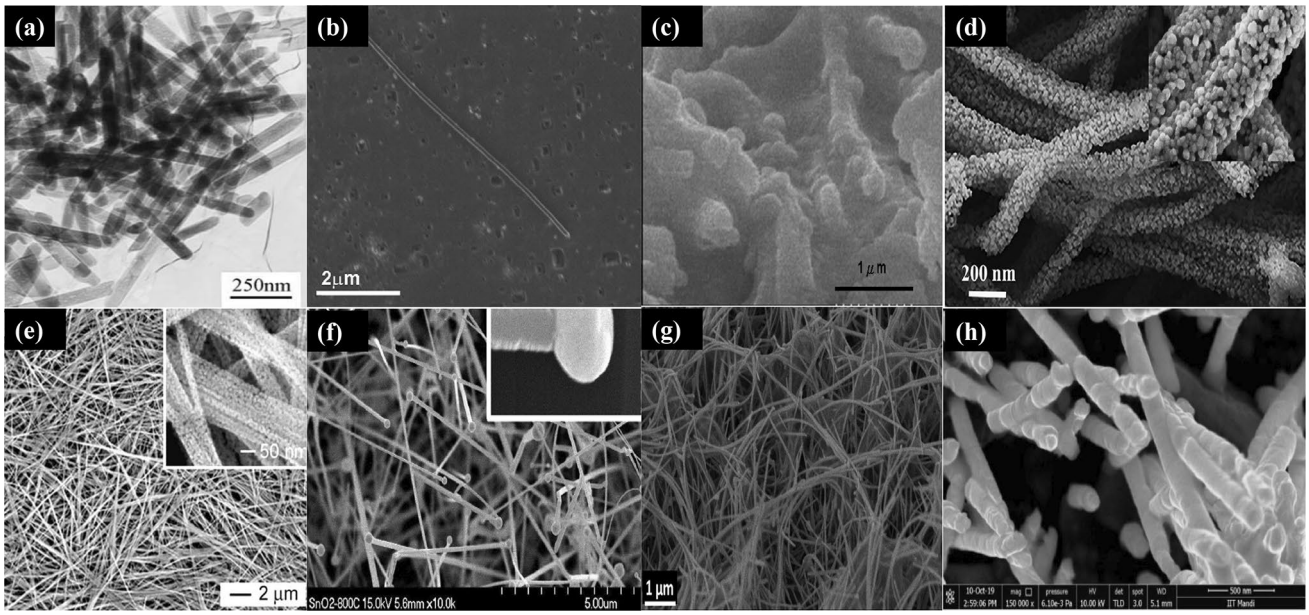

Fig. 6 SEM pictures of **a** SnO_2 nanowires synthesised by co-precipitation method [110], **b** SnO_2 NWs on SiO_2/Si substrate prepared by hydrothermal method [107], **c** ITO nanowire coated by TiO_2 nanotubes prepared by sol–gel method [120], **d** Porous SnO_2 PNWs prepared by electrospinning method [126], **e** SnO_2 NWs prepared at 500 °C by polyol method [130], **f** SnO_2 NWs prepared by CVD method [135], **g** chitosan-deposited SnO_2 NWs prepared by PVD method [140], **h** SnO_2 NWs prepared by electrodeposition method [144]

is ITO-NWs synthesized by Qui et al. The SEM morphology of this composite can be seen in Fig. 6a [110].

2.2 Hydrothermal Method

One of the most popular methods for preparing nanowires is hydrothermal synthesis. It's essentially a solution-reaction-based process. The development of nanomaterials in hydrothermal synthesis will occur throughout a wide temperature range, from room temperature to extremely high temperatures. Moreover, based on the vapour pressure of the main composition of the reaction, either low-pressure or high-pressure conditions may be utilized to regulate the morphology of the materials to be prepared. This method has been used to synthesise a wide range of nanomaterials successfully. Hydrothermal synthesis has several benefits over other methods. At high temperatures, hydrothermal synthesis can produce nanomaterials that are unstable. The hydrothermal approach will create nanomaterials with high vapour pressures with minimal material loss. In hydrothermal synthesis, the compositions of nanomaterials to be synthesised can be well regulated by liquid phase or multiphase chemical reactions [111, 112]. Generally, the high-pressure hydrothermal pressure (HPHS) technique produces inorganic nanomaterials [113]. Here, in the physical experimental setup of the HPHS for the synthesis of nanomaterials.

To begin with, the precursor materials are put in containers with a solid-to-water ratio of approximately 1:10. The enclosed containers are placed in a high-pressure tank that is hermetically sealed and placed in a furnace. An autogenous pressure is generated by applying the desired hydrothermal synthesis temperature. As soon as the autoclave reaches temperature equilibrium, the external pressure is modified. The reaction takes place when the hydrothermal pressure is mounted. Temperature gradients inside the containers must be avoided because they induce convection and, as a result, fluid transfer, which promotes crystal growth after nucleation. Temperature variations in the furnace have similar adverse effects because a higher dissolution rate disturbs the complex equilibrium of dissolution-crystallization, whereas a lower temperature causes more supersaturation. This results in an unintended crystal growth phase instead of the intended nucleation only, depending on the crystal growth rate and, hence, the particular material to be synthesised.

Furthermore, in the normal laboratory set-up, temperature fluctuations mean variations in hydrothermal strain, reinforcing previously observed temperature effects [114]. Physical parameters are important in this method, but chemical aspects are also significant [115]. For example, O. Lupan et al. have synthesised rutile tin oxide nanowires with a cheap and easy fabrication process, the SEM image is illustrated in Fig. 6b [107].

2.3 Sol–Gel Method

The sol–gel method is a well-known synthetic technique for producing high-quality metal oxide nanoparticles and mixed oxide composites. The texture and surface characteristics of the materials could be restrained very well with this approach [116]. With a low process temperature, the sol–gel method may produce a very pure and homogenous layer, controlled porosity and homogenous particle dispersion across a wide region [117]. The sol (or solution) eventually develops a gel-like diphasic structure comprising both a liquid phase as well as a solid phase with morphologies ranging from isolated particles to continuous polymer networks in this chemical process. Precipitation can produce ultrafine and uniform ceramic powders. These powders of single and multi-component composition may be manufactured on a nanoscale particle size [118] for dental and biomedical applications. In the process, mainly five steps are there; hydrolysis, polycondensation, aging, drying, and thermal decomposition. Firstly, raw material is uniformly mixed with liquid phase then, hydrolysis and polycondensation reactions are carried out to form a transparent and stable gel. Afterward, since the aging of sols, colloidal particles increasingly assemble to create gels of three-dimensional network structures. Then, materials with microstructures and even nanostructures can be prepared after different processes such as drying and sintering [119]. There are some merits and demerits of this method, advantages; Products have higher purity, a controllable degree of porosity, are easy to prepare in different sizes, are simple to carry out, and allow for low-temperature synthesis. While disadvantages; Organic solvents have a slower reaction time and are toxic to the human body [119]. In the example, Wand et al. had developed the ITO-NWs (Fig. 6c/SEM) with the help of the sol gel method [120].

2.4 Electro Spinning Method

Electrospinning is one of the best methods to produce metal oxide nanowires because its merits, like Simplicity, greater performance, cheaper, and high reproducibility, are all desirable qualities [121]. A grounded collector, a power source with a high voltage (usually in the kV range), and a metallic needle in a syringe (solid substrate or liquid media) in the processing. A high voltage is spread over to solutions or melts in a traditional electrospinning phase. A pendant droplet emerges as a result. As electrostatic repulsion overcomes the fluid's surface tension, the pendant droplet at the needle's tip deforms into a conical droplet called as the Taylor cone. A well-charged jet of polymer liquid is expelled from the needle's tip as Surface tension is overcome by electrostatic force of the conical droplet. The contact of the electric field with the fluid's surface tension bends the jet

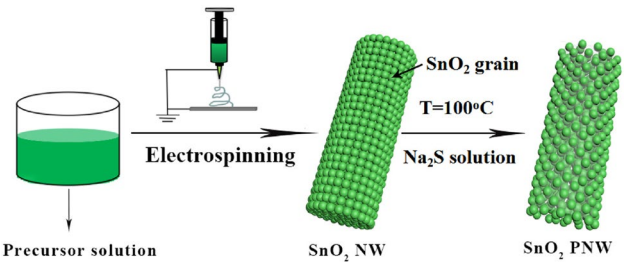

Fig. 7 Schematic representation of synthesis SnO_2 PNWs through electrospinning method [126]

stream and causes it to whip about, causing the solution to evaporate. This allows the jet stream to continually elongate as a thin and long strand, which then solidifies and is finally collected into a grounded collector, forming a uniform fiber. The key drawback of chemically grown NWs is their incorporation on planar substrates to use their useful properties, such as transition and creating contacts, which can be difficult [122–125]. Here, porous tin oxide nanowires had been developed by Z. Lou et al. by utilizing this method, the morphology of this material is depicted in Fig. 6d. Moreover, the schematic representation of this method is elicited in Fig. 7 [126].

2.5 Polyol Technique

In this technique, the polyol process consists of rapid nucleation followed by slow particle growth at high temperature; the precursor is rapidly added at a very high temperature in the vessel containing a complexing solvent such as Polyethylene glycol (PEG) with a high boiling point [127]. In the mechanism, Alkoxides were converted into a chain-like glycolate complex in the majority of situations and then crystallised into uniform nanowires when heated. The use of ethylene glycol to form chain-like complexes with suitable metal cations, which could easily aggregate into 1D nanostructure within an isotropic medium, was crucial to the success of this synthesis. Polyol appears to be a favourable route for making a diverse variety of oxide nanowires [128]. In addition, this method has its merits like stoichiometry control, size dimensions, size distribution, and so on [129]. In the example, Xia et al. has synthesised tin oxide nanowires (for SEM, refer to Fig. 6e) through the polyol method [130].

2.6 Chemical Vapour Deposition (CVD)

Chemical vapour deposition is a frequently used method for the preparation of nanomaterials [131]. The deposition of a solid on a heated surface as a result of a chemical reaction in the vapour phase is known as CVD technique. CVD is an atomistic vapour-transfer method that comes from the

chemical process of gaseous components on a heated substrate to produce a completely dense deposit. Moreover, Chemical vapour deposition (CVD) is a method for creating high-quality, high-performance solid materials. Thin films are often produced using this method in the semiconductor industry [132]. However, the CVD process is defined as the transport of reactant vapour or reactant gas towards a substrate maintained at a high temperature, where the reactant cracks into different products that diffuse on the surface, undergo a chemical reaction at an appropriate site, nucleate, and grow to form the desired material film. There are generally two types of CVD: hot-wall CVD and Cold wall CVD, depending upon the application it's used [133, 134]. In 2018, scientists from the Republic of Korea synthesized, SnO_2nanowires through a thermal CVD process in a reduced hydrogen atmosphere, the morphology can be seen in Fig. 6f [135].

2.7 Physical Vapour Deposition (PVD)

Any type of inorganic substance, such as metals, alloys, and organic materials, may be deposited using physical vapour deposition (PVD) [136]. In addition, sputtering, ion plating, magnetron sputtering, and electron beam sputtering are all examples of PVD. The material layers in the sputtering process can vary from angstroms to millimeters [137]. In the process, using a high-energy ion source in the presence of a vacuum and an inert gas, normally argon, atoms are separated from the target substance in the first phase of PVD. The target substance is exposed to a high-energy source, which causes atoms to vaporise from the surface. The vaporised atom then travels toward the substrate's surface and into the chamber. If the deposited substrate is a metal oxide, carbide, or nitrite, the reaction will occur; otherwise, it will not. The vaporised atoms enter the substrate surface and settle themselves as a thin film there [138]. On the surface of the substrate, the PVD process creates a uniform coating from the nanoscale to the visible size. Almost all inorganic and organic materials and some organic materials can be incorporated using this method. In the PVD phase, less resistance is caused, resulting in a compact layer structure with enhanced mechanical properties such as stiffness and wear resistance due to heterogeneous nucleation. This method has many merits, like almost every kind of Nanocoating or nanomaterial can be prepared by this method. Despite this, one significant demerit is the operating temperature, which is very high for very high vacuums, resulting in increased energy consumption and requiring special operator attention. To remove the high heat loads, a water-cooling system is needed [139].SnO_2 NWs (morphology can be seen in Fig. 6g) are synthesized using a seed-layer-assisted vapour–liquid–solid (VLS) technique, described by Comini et al. [140].

2.8 Electrodeposition Method

The electrodeposition process also referred as electroplating is an electric current-driven technique of deposition that allows meticulous control of epitaxially coating species such as NPs, nanowires, and other materials onto a conductive target substrate [141]. Electroplating and electrophoretic deposition are two forms of electrodeposition (EPD). Electroplating is normally done in an aqueous solution containing ionic compounds, whereas EPD is done in a particle suspension. In electroplating, during the deposition of the metal or oxide layer in the electrode, there is a charge transition. In other words, as an external electric field is applied, positively charged ions in the electrolytic solution are diminished, allowing them to be deposited into a target substrate (cathode). Deposition happens in the EPD without the need for a chemical reaction (reduction) [142]. Some advantages are associated with this method, such as the method will deposit nanostructures and thin films into vast specimen areas of complicated shapes, making it ideal for industrial use. For instance, electrodeposition could be done inside a nanoporous membrane that acts as a blueprint for the growth of NPs, and it would be done at room temperature with water-based electrolytes. It may be reduced down to a few atoms or expanded up to huge dimensions. with film thickness ranging from 1 nm to 10 microns [143]. In the year 2020, S. Arya and his group had synthesised tin oxide nanowires for gas sensing application through template-based electrodeposition technique, the schematic representation of the procedure and SEM analysis can be seen in Figs. 6h and 8 [144].

Figure 9a illustrates the comparative data for methods used to synthesis nanomaterials and their utilization for detecting various hazardous gases. Besides this, Fig. 9b elicits; based on literature statics of the methodologies used for the synthesis of tin oxide nanowires as a chemiresistive gas sensor [78, 145–183].

3 Tin Oxide Nanowires (SnO_2 NWs) as a Gas Sensor

Gas sensors are vital in our daily lives since they detect various gases that are hazardous to human and environmental safety [184, 185]. Gas pollution, food safety assessments, medical procedures for detecting illness in its early stages, human safety (mines and interior applications need volatile and explosive gases), and the automotive and chemical industries are also examples of applications for such sensors [186–192]. Many recent research initiatives in this field have concentrated on developing high-performance sensors capable of providing correct data with high sensitivity [193, 194]. Assessing air quality, for example, is one of the most important duties in many developing nations when it comes to devising new environmental solutions to minimise significant health hazards [195, 196]. As a result, as previously

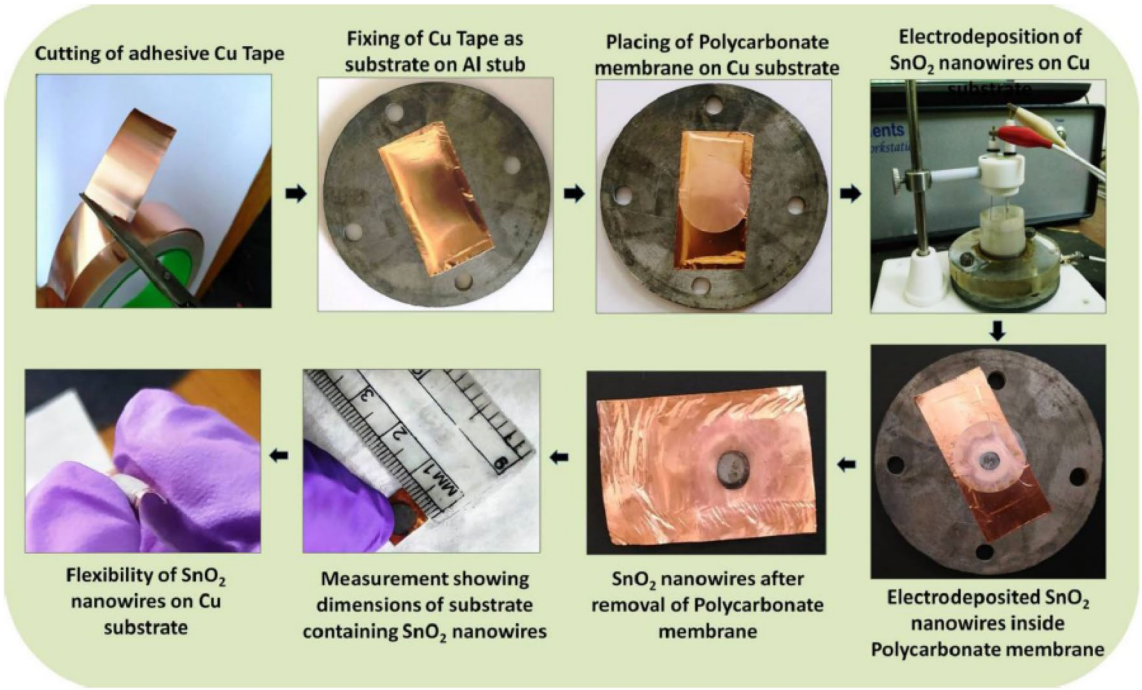

Fig. 8 Experimental procedure to prepare SnO_2 nanowires [144]

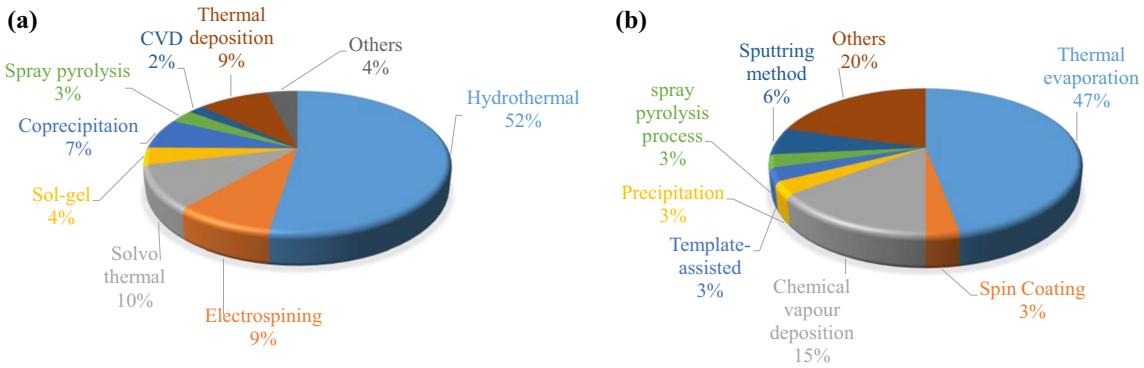

Fig. 9 **a** Percentage distribution of the use of nanomaterial fabrication techniques for hazardous gas sensing application [108]. **b** Based on literature statics of the methodologies used for the synthesis of tin oxide nanowires as a chemiresistive gas sensor [78, 145–183]

said, numerous sensors have been created, with tin oxide nanowire (operating temperature would be RT) being at the top of the list. Figure 10 depicts the list of gases and their sources that must be detected. In addition, Table 4 below illustrates the limitations of dangerous gases and their negative impact on human health. Furthermore, the next part discusses the different tin oxide nanowire gas sensors used for monitoring hazardous and poisonous gases at RT, material properties, and sensor response and recovery time.

As far as we know, there are no more articles found that can exhibit the sensing property at room temperature by using SnO_2 NWs as a gas sensor. However, few papers have been obtained which can provide sensing by the same material at RT. In the following section, individual gases detection has been explained in detail.

3.1 Detection of Oxidising and Reducing Gases Using Tin Oxide Nanowires

3.1.1 Nitrogen Dioxide (NO_2)

This is the type of oxidizing gas, Nitrogen oxides (NO_2 and NO) are dangerous gases manufactured by chemical companies and automobiles. The most dangerous gas is

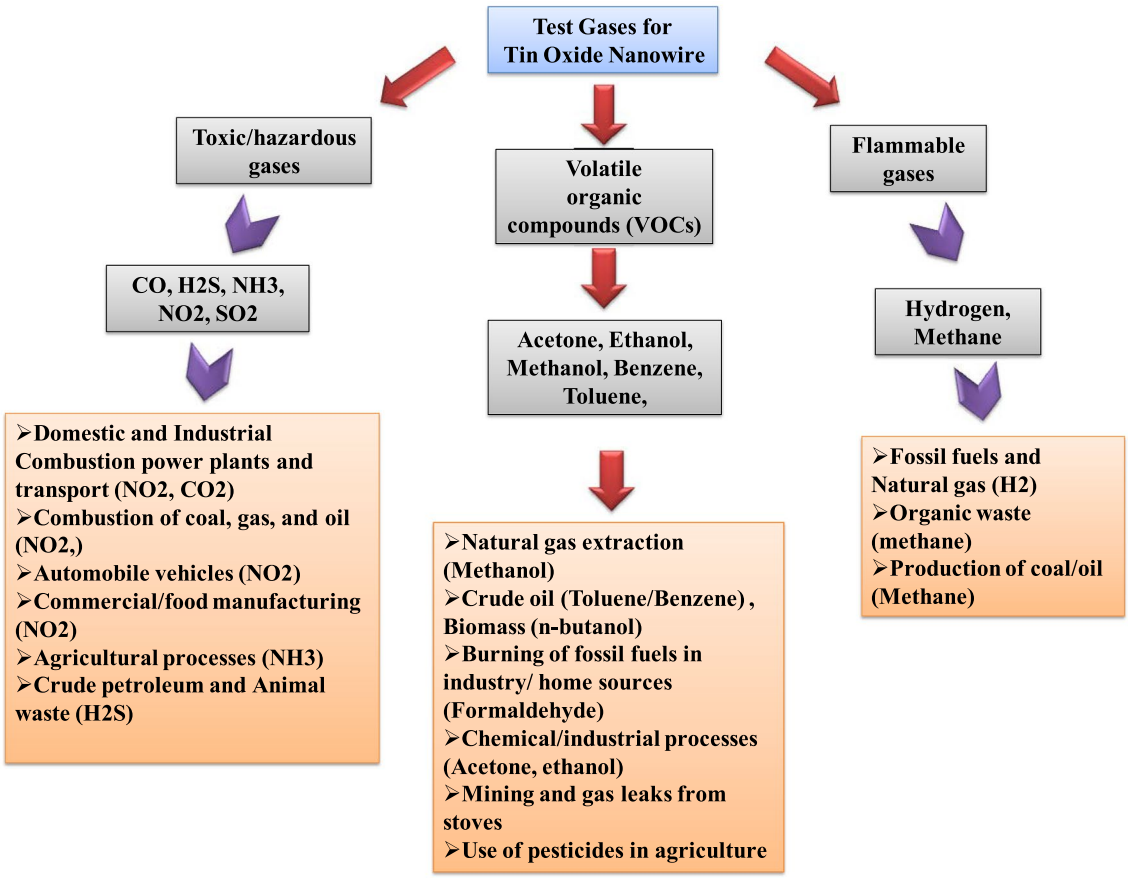

Fig. 10 Distinguish among the type of toxic gases and their sources of production

nitrogen dioxide (NO_2), with a TLV of 3 ppm. NO_2 is also an important component of atmospheric processes that result in ground-level ozone, a major smog component [100, 210]. Nitric oxide (NO, 90–95 percent of total) is the primary component of exhaled air NOx mixes from power plants, with values ranging from 0 to 4000 ppm [211]. Inhaling NO_2 has a major effect on the respiratory system and is highly dangerous to humans because it damages the lungs [212].

Choi et al. and group [145] reported SnO_2 nanowires decorated by insulating amorphous carbon layers for upgraded room-temperature NO_2 gas sensing; they synthesised a-c-decorated SnO_2 NWs through flame carbon vapour deposition method (FCVD). In morphological data, Fig. 11a–c illustrates the SEM images, in which, it was found a-c-SnO_2 NWs had been decorated by nanoparticles like carbon structure, and shells in the material are not uniform. The density of the amorphous surface was not consistent, which would be good in case of sensing because, irregularity in a surface would enhance the adsorption and enlarge the cross-sectional area. Furthermore, Fig. 11d–f shows the TEM pictures of the SnO_2 NWs composite, it elicits the amorphous carbon had been unevenly adsorbed on the smooth SnO_2 surface having a nanoparticle-like shape, among these three TEM images Fig. 11d and f illustrates the bright and dark field modes respectively, which confirms that there is no damage on the structure of SnO_2surface. Then, Fig. 11(h-i) illustrates, on the exposure of NO_2 gas with varying concentration like 2, 4, and, 6 ppm on the bare SnO_2 as well as a-c-SnO_2 NWs gas sensor, through this, comparative responses have been obtained like, at the RT the response by a-c-SnO_2 NWs was 11.2 s, whereas, very low response was received in case of bare SnO_2. Furthermore, Fig. 11j shows the comparison of various gases exposures on the a-c-decorated SnO_2 NWs, with the concentration of 10 ppm and, in this data the highest response (33.41 s) was received in the case of NO_2 gas only as compared to other gases. Park et al. [146] reported SnO_2-Core/ZnO-Shell Nanowires used for the detection of NO_2 Gas at room temperature and under UV-illumination. In which, SnO_2-Core/ZnO-Shell nanowires had been produced by the thermal evaporation of Sn powder, then followed atomic layer deposition of ZnO.SnO_2-Core/ZnO-Shell Nanowires are proven very high sensitivity towards NO_2 gas of low concentration 1–5 ppm at room temperature with responses ranging from ~239 to ~619% (Fig. 11m), in

Table 4 Depicted concentration limit of hazardous gases, impact on human health, and properties

Gas name	TLV	IDLH	Human health issues	Properties	Refs
Acetone	750 ppm	2500 ppm	Muscle weakness, dry mouth, tiredness, dizziness, nausea, and nerve-damaging narcosis are all symptoms of narcosis	Colorless liquid with a strong odour that is used to dissolve plastics in labs as a reagent	[197]
Formaldehyde	0.1–0.3 ppm	20 ppm (OSHA)	At 6 ppm, a human carcinogen causes lung damage and leukaemia in humans (nasopharyngeal carcinoma)	Colorless and combustible	[198, 199]
Ethanol	(1000 ppm-STEL) (ACGIH)	3300 ppm (NIOSH)	Breathing difficulties, eye irritation, sleepiness, and headache	Colorless, flammable, and volatile	[200]
NO_2	0.3 ppm (ACGIH)	13 ppm (NIOSH)	Lung damage, eye irritation, and ozone production	It has a pungent odour and is not combustible	[201, 202]
H_2S	1-5 ppm (ACGIH)	100 ppm (NIOSH)	Highly reactive t with haemoglobin causes olfactory system injury	It smells like a rotten egg, is colourless, and is poisonous	[203–205]
NH_3	25 ppm (ACGIH)	300 ppm (NIOSH)	Hazardous to human skin, eyes, and respiratory systems, as well as caustic and irritating	It's colourless, caustic, and poisonous	[206]
CO	50 ppm (OSHA) and 35 ppm (NIOSH)	1200 ppm (NIOSH)	Headache, loss of consciousness, sudden mortality owing to haemoglobin bind and reduced oxygen transfer, dizziness collapse, and nausea are all symptoms of a haemoglobin bind	Nonirritating, colourless, odourless, tasteless	[207, 208]
H_2	NA	NA	Dizziness, headaches, drowsiness, and nausea, as well as stinging of the nose and throat, vomiting (the pure form is a chemical asphyxiant), dizziness, headaches, drowsiness, and nausea	Metal smelting, tasteless, low minimum ignition energy (0.017 mJ), nontoxic, explosive/ utilised as fuel in automobiles, petroleum extraction, glassmaking	[209]

TLV threshold limit value, *IDLH* immediately dangerous to life or health air concentration, *OSHA* occupational safety health administration, *NIOSH* National institute for occupational safety and health, *ACGIH* American conference of governmental industrial hygienists

contrast, pure SnO_2 and ZnO nanowires showed responses ranging from ~126 to ~180% and from ~102 to ~104%, respectively. Apart from this, the SEM image (Fig. 11k) reveals the diameter of 50 to 250 nm and length is few to few tons in µm of the composite nanowire. Moreover, the EDX analysis has been illustrated in Fig. 11l, in which the elements of the composite were confirmed such as Sn, Zn, and, O. Other, sensors based on tin oxide nanowire provide sensing at RT are depicted in Table 5.

The reaction mechanism for the NO_2 sensing would be stated as:

$$NO_{2(gas)} + e^- \rightarrow NO^{2-}_{(ads)} \quad (5)$$

$$NO^{2-}(ads) + O^-(ads) + 2e^- \rightarrow NO\,(gas) + 2O^{2-}(ads) \quad (6)$$

3.1.2 Chlorine (Cl_2)

Chlorine (Cl_2), a very poisonous gas with a strong odour, is largely employed in cleansing of water, pulp bleaching in paper mills, pesticide manufacturing, and chemical and pharmaceutical sectors; as a result, the risk of Cl_2 exposure is considerable [213]. Cl_2 molecules can combine with water in the lung mucosa to create hydrochloric acid when exposed to Cl_2 gas by inhalation; As a result, even a few deep breaths of 1000 parts per million (ppm) Cl_2 can be fatal to humans. Furthermore, low-level Cl_2 exposure might exacerbate respiratory diseases and make the eyes itch [214]. The human nose detects Cl_2 gas odour at concentrations of 0.1–0.3 ppm, while the workplace exposure limit for Cl_2 is around 34 parts per billion (ppb) [215]. As a result, a very sensitive gas sensor capable of detecting Cl_2 gas at the parts-per-billion (ppb) or parts-per-trillion (ppt) level must be created for applications such as environmental surveillance, leakage detection, and safe usage [216–218].

In the year 2010, Sen et al. [151] reported at room temperature Cl_2 and H_2S detected by the SnO_2 nanowire, its produce by the thermal evaporation method. Cl_2 gas detected 6 ppm concentration with response time 100 s and recovery time is very slow 40 min (Table 5). Van Dang et al. [153] reported Cl_2 gas sensing using ZnO, WO_3, and SnO_2 nanowire sensors, had been fabricated using an on-chip growth technique with chemical vapour deposition (CVD). The results showed that SnO_2 nanowires were more sensitive to Cl_2 gas than ZnO and WO_3 nanowires. In characterization portion, The SEM picture of the SnO_2 sample (Fig. 12a) revealed a homogeneous shape and the presence of long nanowires with an average diameter of

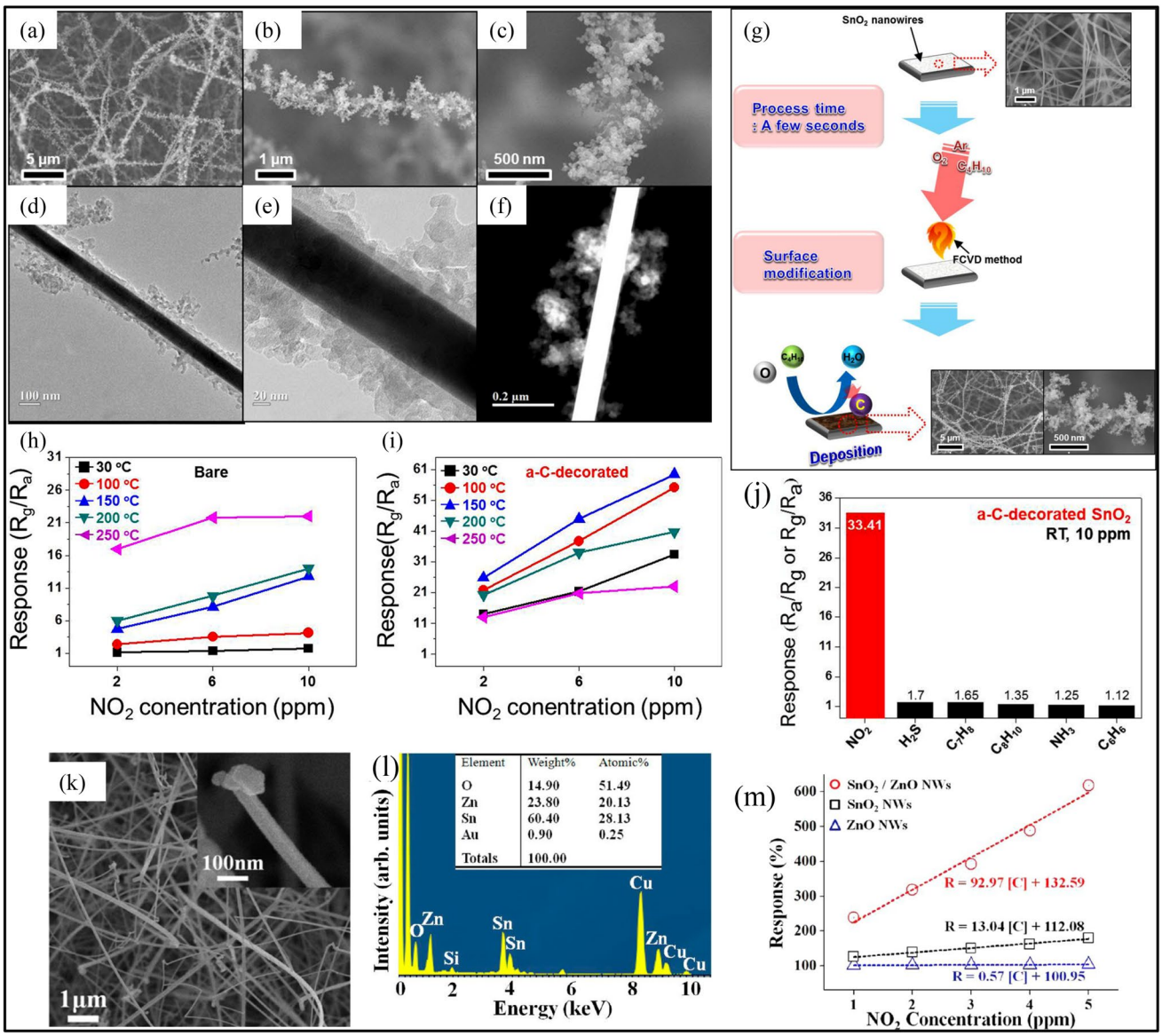

Fig. 11 **a**–**c** SEM pictures of a-C-decorated (5 s) SnO_2 NWs at low and high magnification. Bright-field and dark-field TEM pictures of the a-C shell produced on SnO_2 NWs (**d**, **e**), **g** The a-C-decorated SnO_2 composite is synthesised, Sensor responses of **h** naked SnO_2 and **i** a-C-decorated (5 s) SnO_2 with variable NO_2 concentration and operation temperature, the gas concentration was varied between 2, 6, and 10 ppm. When the exposure duration to NO_2 gas reached 500 s, the response values were obtained, **j** At 24 °C, selectivity pattern of a-C-decorated (5 s) SnO_2 to 10 ppm of specified gases, **k** SEM image of SnO_2-Core/ZnO-Shell Nanowires, **l** EDX analysis of SnO_2-Core/ZnO-Shell Nanowires, **m** Response vs concentration graph for the three nanowires based on tin oxide [145, 146]

80 nm and a length of a few micrometres. Then, The HRTEM picture of a SnO_2 nanowire (Fig. 12b) revealed distinct lattice fringes with an interspace of 0.26 nm, which corresponded to the distance between (101) planes of tetragonal SnO_2, allowing the growth direction to be identified as < 101 > [32].Further, from Fig. 12e it can be seen that, chlorine gas detected at 50 °C, with the concentration of 2.5 ppm the response was received 130 s. Besides this, the selectivity of the Cl_2 gas was found to be highest in case of sensing by SnO_2 NWs as illustrated in Fig. 12g. In addition, the design of identical sensor is depicted in Fig. 12c, while a micro-heater and a pair of Pt/Cr electrodes were included on the sensor chip (Fig. 12d). Dry etching was used on the rear side of the Si wafer to lower the device's power consumption. Besides this, as per the Fig. 12f, the response and recovery time was approximately 230 s and 260 s respectively, for the Cl_2 sensing at room temperature. Apart from this, the highest response towards chlorine gas confirmed by tin oxide nanowires at RT (Fig. 12h). In the year 2010, Sen et al. [154] prepared $SnO_2/W_{18}O_{49}$ nanowire hierarchical heterostructure by the thermal evaporation of

Table 5 SnO_2 nanowires as Chemiresistive gas sensor for various gases at room temperature

Material	Synthesis method	Selective against	Analyte gas	Concentrations of gages (ppm)	Operating temp. °C	Response(Ra/Rg) or (Rg/Ra)* or $[(R_a - R_g/R_a) \times 100]$**	Resp. /Reco.time (s/s)	Refs
Carbon-decorated SnO_2 NWs	Carbon vapour deposition method	NO_2, H_2S, C_7H_8, C_8H_{10}, NH_3, C_6H_6	[a]NO_2	2	RT	13.99*	NR	[145]
				6	RT	21.35*	NR	
				10	RT	33.41*	NR	
			H_2S	10	RT	1.7	NR	
			C_7H_8	10	RT	1.65	NR	
			C_8H_{10}	10	RT	1.35	NR	
			NH_3	10	RT	1.25	NR	
			C_6H_6	10	RT	1.12	NR	
SnO_2 NWs	Thermal evaporation	NO_2	[a]NO_2	5	RT	~ 126 to ~ 180**	90/220	[146]
SnO_2-Core/ZnO-Shell NWs	Followed by layer deposition of ZnO on SnO_2 NWs	NO_2	[a]NO_2	1–5	RT	~ 239 to ~ 619**	100/220	[146]
SnO_2 NWs	Thermal evaporation	NO_2	[a]NO_2	10 to 100	RT	~ 85**	< 15 min./30 min	[147]
SnO_2 NWs	–	NO_2, SO_2, NH_3, H_2, acetone, ethanol	[a]NO_2	2	RT	1.8*	NR	[148]
			SO_2	2	RT	1.0*	NR	
			NH_3	2	RT	1.1	NR	
			H_2	2	RT	1.0	NR	
			acetone	2	RT	1.0	NR	
			ethanol	2	RT	1.0	NR	
He^+ irradiated SnO_2 NWs	SnO_2 nanowires were irradiated with an ion beam	NO_2, SO_2, NH_3, H_2, acetone, ethanol	[a]NO_2	2	RT	14.2*	292/228 s	[148]
			SO_2	2	RT	1.1	NR	
			NH_3	2	RT	1.3	NR	
			H_2	2	RT	1.1	NR	
			acetone	2	RT	1.0	NR	
			ethanol	2	RT	1.0	NR	
SnO_2 NWs	Thermal evaporation	NO_2	[c]NO_2	10–50	RT	12*	590/1850s	[149]
Ru-doped SnO_2 NWs	–	NO_2, LPG	$PRENO_2$	50	RT	35*	3/39–90 s	[150]
SnO_2 NWs	Thermal evaporation	Cl_2, H_2S	Cl_2	6	RT	65–75**	100 s/40 min	[151]
SnO_2 NWs	Thermal evaporation		H_2S	7	RT	125**	170/550 s	[151]
SnO_2 NWs/rGO	Spin Coating	H_2S, NH_3, SO_2, NO_2, Ethanol	[a]H_2S	50	RT	33	2/292	[152]
SnO_2 NWs	Chemical vapour deposition	Cl_2, CO, H_2S, ethanol, NH_3	[a]Cl_2	50 ppb	RT	57*	10 to 285/8 to 265 s	[153]
$SnO_2/W_{18}O_{49}$ NWs	Thermal evaporation	Cl_2	Cl_2	6	RT	11.0*	4.6/17 min	[154]
SnO_2 NWs	Precipitation	CO, Ethanol	CO	20	RT	4	NR	[155]
			Ethanol	6000	RT	8000	NR	[155]
Ar/O_2 and H_2O Plasma treated SnO_2 NWs	Chemical vapour deposition	CO, Benzene	[a]CO	100	RT	9**	NR	[156]
Pd-doped SnO_2 NWs	Thermal evaporation	H_2	H_2	1000	RT	44	NR	[157]

Table 5 (continued)

Material	Synthesis method	Selective against	Analyte gas	Concentrations of gages (ppm)	Operating temp. °C	Response(Ra/Rg) or (Rg/Ra)* or [$(R_a - R_g/R_a) \times 100$]**	Resp. /Reco.time (s/s)	Refs
SnO_2 NWs	Thermal evaporation	H_2	H_2	1000	RT	1.7	1.3 min/0.9 min	[158]
Pt-doped SnO_2 NWs	Thermal evaporation	H_2	H_2	1000	RT	–	1.7 min/21.7 min	[158]
Pd-doped SnO_2 NWs	Thermal evaporation	H_2	H_2	1000	RT	43.8	2.3 min/95.5 min	[158]
SnO_2 NWs	Thermal evaporation	H_2	H_2	500	RT	4	10 s	[159]
SnO_2 NWs	Template-assisted	–	Nitrobenzene	73–2490 ppb	RT	5–20**	NR	[78]
			Ethanol	15.6	RT	2.2**	NR	
Pt doped SnO_2 NWs	Template-assisted	Ethanol, Methanol, Isopropanol, Acetone Chloroform, Ethyl Acetate	Ethanol	15.6	RT	57.1**	NR	[78]
			Methanol	17.4	RT	45**	NR	
			Isopropanol	15.8	RT	65**	NR	
			Acetone	16.6	RT	32	NR	
			Chloroform	17.8	RT	40	NR	
			Ethyl Acetate	17.1	RT	38	NR	
Cu doped SnO_2 NWs	Template-assisted	Ethanol, Methanol, Isopropanol, Acetone Chloroform, Ethyl Acetate	Ethanol	15.6	RT	20.8**	NR	[78]
			Methanol	17.4	RT	20**	NR	
			Isopropanol	15.8	RT	18**	NR	
			Acetone	16.6	RT	20	NR	
			Chloroform	17.8	RT	10	NR	
			Ethyl Acetate	17.1	RT	25	NR	
In doped SnO_2 NWs	Template-assisted	Ethanol, Methanol, Isopropanol, Acetone Chloroform, Ethyl Acetate	ethanol	15.6	RT	45.3**	NR	[78]
			Methanol	17.4	RT	30**	NR	
			Isopropanol	15.8	RT	45**	NR	
			Acetone	16.6	RT	21	NR	
			Chloroform	17.8	RT	9	NR	
			Ethyl Acetate	17.1	RT	28	NR	
Ni doped SnO_2 NWs	Template-assisted	Ethanol, Methanol, Isopropanol, Acetone Chloroform, Ethyl Acetate	ethanol	15.6	RT	57.2**	NR	[78]
			Methanol	17.4	RT	40**	NR	
			Isopropanol	15.8	RT	55**	NR	
			Acetone	16.6	RT	30	NR	
			Chloroform	17.8	RT	10	NR	
			Ethyl Acetate	17.1	RT	20	NR	

[a]Highly Selective Gas for Sensor, *N.R* not reported, *Ra*/*Rg* (for reducing gases) or *Rg*/*Ra* (for oxidizing gases)

Sn in a horizontal tubular furnace. This sensor showed high selectivity and good response towards detection of Cl_2 gas at room temperature. The Sensor detected 0.25 ppm and 6 ppm concentration of Cl_2 with response ($S = I_g/I_a$) ~ 1.1 and 11.0, respectively. The response and recovery times for 6 ppm Cl_2 are found to be 4.6 min and 17 min, respectively (Table 5). The possible sensing mechanism of Cl_2on SnO_2 is given as [154]:

$$1/2Cl_2 + O^{2-}_{(ads)} \rightarrow Cl^-_{(ad)} + 1/2O_2 + e^- \quad (7)$$

$$1/2Cl_2 + O^{-2}_{O} \rightarrow Cl^-_{O} + 1/2O_2 + e^- \quad (8)$$

$$1/2Cl_2 + e^- \rightarrow Cl^-_{ad} \quad (9)$$

$$1/2Cl_2 + e^- + V_O \rightarrow Cl^-_{O} \quad (10)$$

3.1.3 Hydrogen Sulphite (H_2S)

The most hazardous manure gas, hydrogen sulphide (H_2S), because it interacts chemically with blood haemoglobin and inhibits oxygen from reaching the body's essential

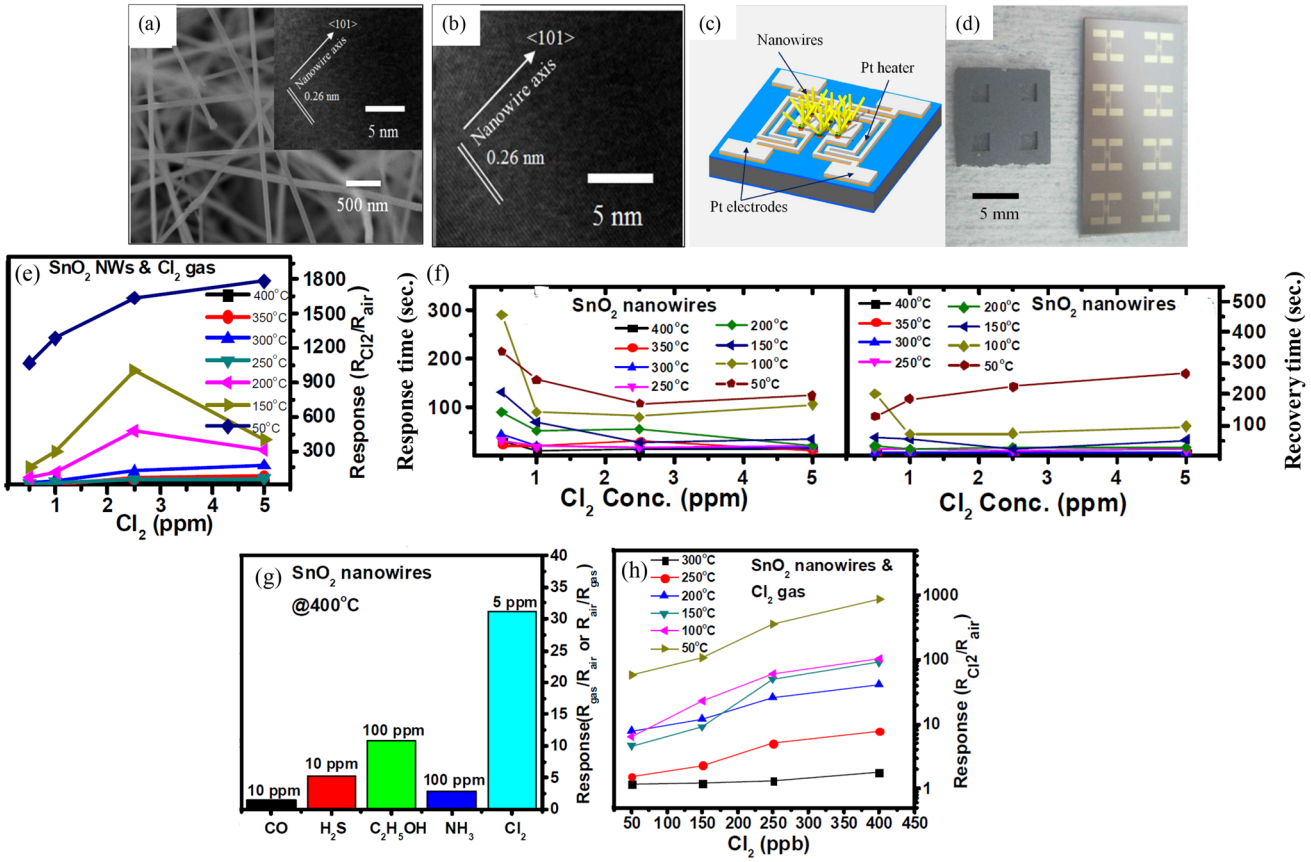

Fig. 12 **a** SEM picture of SnO_2 utilised to detect Cl_2 gas, **b** TEM picture of SnO_2 nanowire utilised for Cl_2 gas sensor detection, **c** The creation of a nanowire sensor chip, **d** Optical representation of a chip array, **e** SnO_2 NWs response to Cl_2 gas at 50 ppb concentration at 50 °C, **f** Response and recovery time of tin oxide nanowire at various temperatures towards chlorine gas, **g** Sensor selectivity to various gases evaluated at 400 °C (CO, H_2S, Ethanol, and NH_3), **h** The sensor response as a function of Cl_2 concentrations observed at various temperatures [153]

organs and tissues, it is classified as a chemical asphyxiant [91, 155, 219–222]. Sen et al. reported the synthesis of tin oxide nanowire by thermal evaporation method for the sensing of H_2S gas at the room temperature. Apart from this, the sensor response towards H_2S gas was at room temperature with 2 ppm concentration only [151]. Moreover, Leu et al. reported nanocomposite of SnO_2 nanowire incorporated with reduced graphene oxide rGO gas sensor for the detection of H_2S gas at room temperature, the sensor was synthesised by one step colloidal synthesis system followed by spin coating on the ceramic substrate for the fabrication of sensor (Fig. 13h). First, in the morphology of the material, HRTEM analysis of SnO_2/rGO nanocomposite has been depicted in Fig. 13a–c, images were taken after 3, 6, and 8 h of reaction time, from this data it could be confirmed that as the reaction time during synthesis increased the precise tetragonal crystalline structure of the material received. Through, SAED pattern, the clear indication of proper distribution and binding of SnO_2 NWs on the surface rGO would observe. When, SnO_2/rGO nanocomposites prepared at three different time intervals. The highest response received by the sensor prepared after 8 h of reaction time upon the exposure of 50 ppm H_2S gas at 22 °C, the response was 33 and time for that was 2 s (Fig. 13d). Apart from this, Fig. 13e, illustrates the response of sensor at various concentrations of the H_2S gas at same temperature conditions, highest response was obtained as the concentration of the H_2S gas surged. Further, when the different analytes have been taken to know the sensing response by the sensor SnO_2/rGO nanocomposite, the maximum response received for the H_2S gas as compared to other gases (Fig. 13f). Besides this, Fig. 13g indicates the response vs time graph for obtaining the three-sensor response such as, SnO_2/rGO, SnO_2, and rGO. Since, the optimum morphology could be seen for the SnO_2/rGO nanocomposite, the greater response (33 at 22 °C, 50 ppm H_2S) was also received by the same [152]. The possible sensing mechanism of H_2S on SnO_2 is given as [100]:

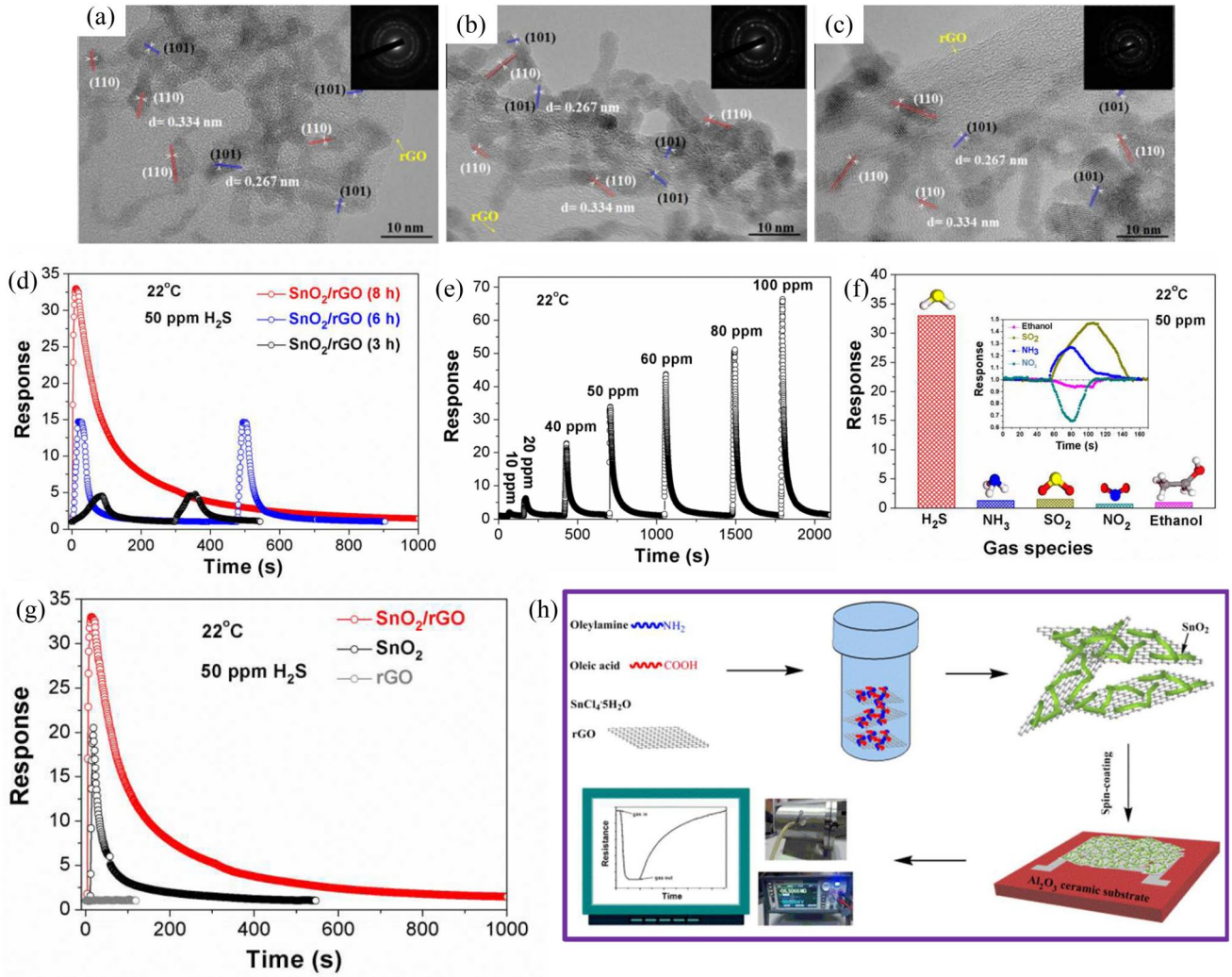

Fig. 13 HRTEM images and SAED patterns of SnO_2/rGO nanocomposites (**a**, **b**, and **c**), which were synthesised at 180 °C for 3, 6, and 8 h, respectively, **d** Gas sensor response curves for varying reaction times based on SnO_2/rGO nanocomposites produced at 180 °C, **e** Response curves for various H_2S concentrations, **f** the ideal gas sensor's selectivity using SnO_2/rGO nanocomposites (8 h), **g** Gas sensor response curves using pure rGO, SnO_2 quantum wires (8 h), and SnO_2/rGO nanocomposites (8 h), **h** The one-step synthesis of SnO_2 quantum wires/rGO nanocomposites, followed by their sensor fabrication and gas sensing test [152]

$$H_2S + 3O^-_{(ads)} \rightarrow H_2O + SO_2 + 3e^- \quad (11)$$

$$H_2S + 3O^{2-}_{(ads)} \rightarrow H_2O + SO_2 + 6e^- \quad (12)$$

3.1.4 Carbon Monoxide (CO)

Carbon monoxide (CO) is a lethal gas that is colourless and odourless that humans cannot detect. It is produced when fuels are burnt inefficiently. It is frequently discovered in automobile exhaust fumes. It has been proven that the gas may bond forever to the iron core of haemoglobin, the oxygen transport protein in the blood. Because of the irreversible binding, oxygen cannot be absorbed, resulting in reduced cellular respiration and death from high levels of CO exposure [100]. Wang et al. [155] reported for the sensing of CO gas detection at room temperature by polycrystalline SnO_2 nanowire, Which is typically synthesised, $SnC_2O_4{\cdot}2H_2O$ had been combined with poly(vinylpyrrolidone) (PVP) in ethylene glycol (EG), followed by refluxing at 195 °C for 3 h. SnO_2 NWs can be detected 20 ppm concentration of CO gas with 4% sensor response [100]. Furthermore, Fisher et al. reported the CO sensing gas sensor based on tin oxide nanowire plasma treated by Ar/O_2 and H_2O. This material has been developed by chemical vapour deposition method. The SEM analysis of the SnO_2 NWs is depicted in Fig. 14a–d, the growth of nanowires prepared via CVD method can be

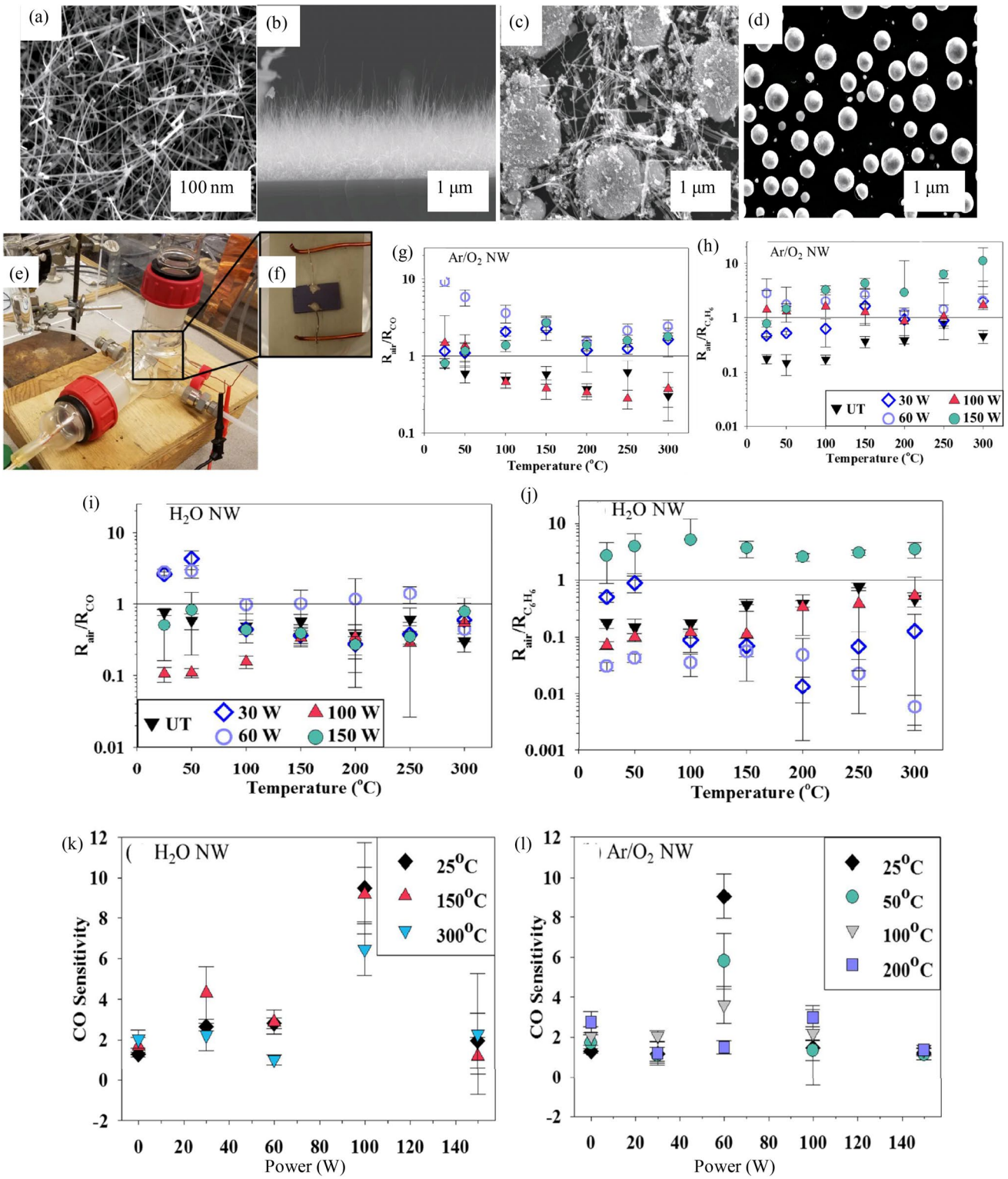

Fig. 14 SEM pictures of **a** SnO_2 CVD produced nanowires and **b** a cross-section of SnO_2 nanowires on ZrO_2 substrates, **c**, **d** H_2O plasma (145 mTorr 150 W, 5 min) treated SnO_2 nanowires (mag 4000X) [223], **e** a snapshot of the full arrangement, and **f** a photo of a sensor attached to the substrate heater's copper leads, **g**, **h** SnO_2 NWs treated gas sensor responsiveness For CO and C_6H_6 gas, Ar/O_2 is used, **i**, **j** Gas sensor response for CO and C_6H_6 gases in SnO_2 NWs treated with H_2O. **k**, **l** Sensitivity of treated H_2O and Ar/O_2 sensors to CO gas for SnO_2 NWs at different temperatures [156]

seen in Fig. 14a, in which the uniform distribution would be observed. Then, the cross sectional view of the SnO_2 NWs on ZrO_2 substrate could be observed in Fig. 14b, fine crystal structure may be detected. While, the unique morphology obtained in case of treated SnO_2 NWs via H_2O, two different magnification images can be seen in Fig. 14c and d. The gas sensing system is shown in Fig. 14e, with the flow of gas through the unit kept at 15 sccm by a flow meter. Then, as shown in Fig. 14f, hand-assembled sensors were made by connecting electrodes of silver wire (1 cm long, 0.25 mm diameter) were attached to SnO_2 substrates with enough silver conductive paste to cover the electrode end (1–2 mm diameter). Further, Fig. 14g and h shows the gas sensor response of SnO_2 NWs by treated with Ar/O_2 for the sensing of CO and C_6H_6 gas, the optimum response was obtained in case of CO gas sensing as compared to C_6H_6. Similarly, the same results in terms of sensor response were obtained in case of SnO_2 NWs treated by H_2O (Fig. 14i, j). The sensitivity for the CO sensing by SnO_2 NWs treated with $Ar/O_2$and H_2O at various temperatures can be seen in Fig. 14k and l [156, 223]. The possible reaction mechanism of CO sensing by SnO_2 is elicited below:

$$CO + O^{-}_{(ads)} \rightarrow CO_2 + e^{-} \quad (13)$$

$$CO + O^{2-}_{(ads)} \rightarrow CO_2 + 2e^{-} \quad (14)$$

3.1.5 Hydrogen (H_2)

Because of the introduction of H_2 as a fuel to support renewable energy, monitoring of H_2 has been increasingly essential in recent years in order to keep its concentration in the atmosphere below 4%. (Beyond which it explodes) [157]. in the year 2013, Shen et al. also reported Pd-doped SnO_2 nanowire for the detection of the H_2 gas at room temperature. This work demonstrated Pd-doped SnO_2 nanowire, Pt-doped SnO_2 nanowire and undoped SnO_2 nanowire at room temperature for detection of H_2. In addition, the response of the undoped nanowire sensor grows from 0.1 to 1.0 when the concentration of H_2 gas rises from 100 to 1000 ppm. The responsiveness of the 2 wt% Pt-doped or Pd-doped nanowire sensors is considerably improved. The response of the 2 wt% Pd-doped nanowire sensor surges from 1.7 to 43.8 as the H_2 gas concentration increases from 100 to 1000 ppm, which is several tens of times that of the undoped nanowire sensor under the same conditions [158]. Apart from this, Yamazaki et al. reported Pd-doped SnO_2 NWs for the H_2 sensing at room temperature through thermal evaporation method. In the morphology of the material, first, Fig. 15a illustrates the FESEM image of SnO_2 NWs which was undoped in nature, it elicits the diameter of wire was 30–200 nm and lengths in micrometer. Then, Figs. 15b and c depicted the TEM and HRTEM analysis of undoped SnO_2 NWs subsequently, In the HRTEM image it was found that nanowire consists the single crystal structure, confirmed by the SAED pattern in which the tetragonal structure was seen at the (110) pattern. Similarly, TEM and HRTEM analysis of 2 wt% Pd-doped SnO_2 nanowire indicates that diameter of the wire reduced in comparison with undoped SnO_2 nanowire, and clearly seen the crystalline structure of it (Fig. 15d, e). Thermal evaporation of tin granules produced SnO_2 nanowires on oxidised Si substrates. Gas sensors were constructed by dropping a few drops of ethanol suspended in nanowires onto oxidised Si substrates with a pair of 100 nm thick interdigitated Pt electrodes, DC sputtering was used to deposit Pt electrodes with 15 fingers and a gap length of 0.12 mm. Figure 15f shows a schematic diagram of a SnO_2 nanowire gas sensor device and the fabrication method. Besides this, Gas sensors were made using SnO_2 nanowires that were undoped, 0.8 wt% Pd-doped, and 2 wt% Pd-doped. With rising Pd concentrations, the sensor response increased. At 100 °C, the 2 wt% Pd-doped SnO_2 nanowire sensor had a response of 253 for 1000 ppm H_2 gas (Fig. 15g).Since, the H_2 is reducing gas the resistance will decrease, here, Fig. 15h–j depicts the resistance vs time graph for the H_2 gas at concentration of 1000 ppm and at the temperature difference of 100 °C and RT. Furthermore, Deshpande et al. [159] reported SnO_2 nanowire synthesis by thermal evaporation method and used MEMS (Micro-electron mechanical device) which used for the detection of H_2 gas at room temperature, in this work the concentration was used from 300 to 1000 ppm, but quick response time was received at 500 ppm and that was 10 s and the sensitivity was approx. 4, Here, generally sensitivity of the sensor would be low because of the room temperature detection like, the O^{2-} ads ions are adsorbed instead of O^{-} ads ions on the SnO_2 surface. O^{-2}ads ion being less reactive species with H_2 than O^{-} ads ions result in lowering the sensor sensitivity towards hydrogen. The reaction mechanism has been illustrated below [159]. Other SnO_2 NWS gas sensors sensing of H_2 at RT are depicted in Table 5.

$$H_2 + 1/2O^{-}_{2(ads)} \rightarrow H_2O_{(ads)} + e^{-} \quad (15)$$

$$H_2 + O^{-}_{2(ads)} \rightarrow H_2O_{(ads)} + e^{-} \quad (16)$$

3.2 Detection of Volatile Organic Compounds (VOCs) Using Tin Oxide Nanowires

Volatile organic compounds (VOCs) are gases that can be expelled from both indoor and outdoor sources; the proportion of VOCs in the indoor unit is higher than in the outdoor

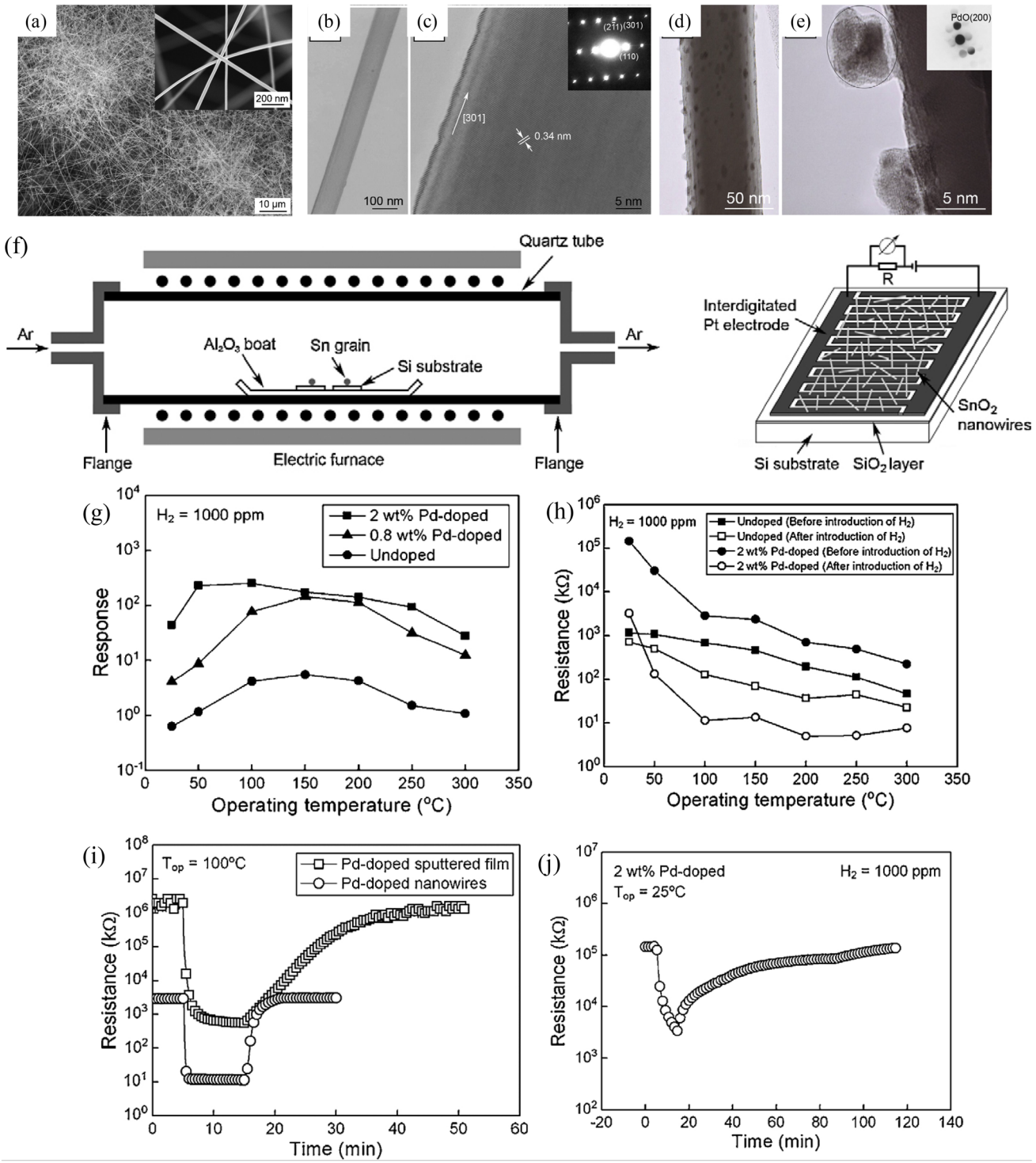

Fig. 15 **a** Undoped SnO_2 nanowires in a typical FESEM picture. **a** TEM picture of an undoped SnO_2 nanowire with a diameter of 95 nm, with an inset of a similar high magnification FESEM image, **b** TEM image of an undoped SnO2 nanowire with a diameter of 95 nm. **c** HRTEM picture of this nanowire and the SAED pattern that corresponds. **d** TEM picture of a 2 wt% Pd-doped SnO2 nanowire with an 80 nm diameter, **e** HRTEM image of the same nanowire. The micro beam diffraction pattern for a single dark spot is shown in the inset. **f** Schematic depiction of a SnO_2 nanowire gas sensor device and schematic design of the equipment used to synthesise SnO_2 nanowires, **g** at various operating temperatures, responses of undoped and Pd-doped SnO_2 nanowire sensors to 1000 ppm H_2 gas, **h** Operating temperature dependency of resistances for undoped and 2wt% Pd-doped SnO_2 nanowire sensors before and after 1000 ppm H_2 gas introduction, **i** Resistance changes in a 2 wt% Pd-doped nanowire sensor and a porous Pd-doped film sensor after exposure to 1000 ppm H_2 gas at 100 °C. **j** At room temperature, the resistance of the 2 wt% Pd-doped SnO_2 nanowire sensor changes when exposed to 1000 ppm H_2 gas [157]

unit [224–226]. These gases can be produced when tobacco, coal, wood, and kerosene are burnt. Cleaning chemicals, dry cleaning oil, paints, lacquers, varnishes, hobby equipment, and copying and printing machines can all emit VOCs, as can perfume and hair gel. Furthermore, VOCs are a class of compounds that can cause eye, nose, and mouth irritation, as well as headaches, nausea, vomiting, dizziness, and skin problems. At greater quantities, the lungs, liver, kidneys, and CNS system might become irritated. Long-term exposure can be harmful to organs including the liver, kidneys, and central nervous system [227]. Because of these disadvantages of these gases, gas sensors are particularly important in measuring VOC vapours.

In the year 2011, Gu et al. reported the synthesis of tin oxide nanowire with various dopant like copper, nickel, platinum as a chemiresitive gas sensor. First, the core nanowires were produced by the use of template-based synthesis. The Fig. 16a shows the SEM image of as produced nanowires, then it will undergo the process of sensor chip assembly or dielectrophoresis (DEP) where, the suspension of nanowire was prepared by the use of solvent ethanol. Further, the substrate was taken that having the electrodes on top which combined with the nanowire suspension. Then after, the solvent was evaporated followed by the development of metallic nanowire. However, the prepared nanowires are inactive so, for the activation oxidation process was carried out through which aligned and oxidized nanowires were received as shown in SEM Fig. 16c. The schematic representation of the DEP process has been illustrated in Fig. 16b. In addition to this, to know the dopant proportion an energy dispersive X-ray spectroscopy (EDS) was performed and obtained the amount percentages of metals present in the tin oxide nanowire like 1% for Pt, 8% copper, 3.5% for In, and 2.4% for Ni. Apart from this, in the measuring of gases first, acetone, as per Fig. 16f the concentration of acetone was taken 800 ppm and the highest response was received by the Pt-SnO_2 NWs far better than core SnO_2 NWs. Second, nitrobenzene, tin oxide nanowires which can detect vapour of nitrobenzene at room temperature (RT) with the concentration of 73 to 2490 ppb, Fig. 16e shows the response by the different doped material on SnO_2 NWs with the different concentration of nitro benzene, the highest response was received by the platinum doped tin oxide nanowire. Moreover, Fig. 16g shows the detection response of the various VOCs gases by the use of dopant and core tin oxide nanowires. When the methanol was exposed on the sensors with varies concentration like 2.9 ppm, 8.7 ppm, and 17.4 ppm, the highest response was obtained by the Pt doped tin oxide nanowire with − 0.4 response at 17.4 ppm concentration. While, acetone was exposed with various concentrations as depicted in Fig. 16g right side corner top, the same sensor gave the highest response of − 0.4.1. Despite this, when ethanol was contacted with 4 types of sensors, similar responses received by Pt-SnO_2 NWs, and Ni-SnO_2 NWs which is approximately − 0.55 at 15.6 ppm concentration. Besides this, very low detection seen in case of chloroform vapours as seen in Fig. 16g middle right. Another two gases have detected by the same sensors which are iso-propanol and ethyl acetate the responses received were − 0.61 and − 0.35 respectively by the Pr-SnO_2 NWs. Overall, it can be commented that platinum doped tin oxide nanowires show the optimum response as compared to other doped and core tin oxide nanowire. The detection of these all gases has been operated at room temperature (RT) [78].

4 Conclusion

All in all, it can be concluded that, nowadays, considerable progress has been accomplished in recent years in lowering the working temperature of SnO2 nanowire-based gas sensors to room temperature, as briefly described in Table 5. The tin oxide nanowire as a gas sensor with high pore sizes, great surface-to-volume ratio, and high density are useful for enhancing the sensing property of SnO2 NWs. This can be achieved by the modifications such as the use of UV or visible light irradiation and doping by various metals. Moreover, as discussed no brief review on this topic has been published yet. Here, the article scope depicts the various synthetic approaches for the fabrication of tin oxide nanowires and their application as a gas sensing property; outlined data have been taken from different reported articles based on SnO2 nanowires. In this review, the main focus has been devoted to the characteristics of SnO2 NWs and its application of sensing different chemical gases such as oxidizing, reducing, and VOCs, with having sensor response at room temperature (RT). According to our findings, the flexibility of tin oxide nanowires using different synthesis techniques is the primary benefit for use in gas sensing and other applications. As earlier mentioned, sensors based on ceramic, pure metal, polymer, and to a name of a few are operated at very high temperature and that leads to high power consumption, high costing, less stability as well as life expectancy. Therefore, to remove these complications gas sensors based on metal oxide 1D materials should be used, particularly reveals response at RT.

5 Future Perspectives

Upon surveying the limitations of the tin oxide nanowire as a room temperature gas sensor, we identified those mainly related to the selectivity and working temperature of the sensor. For increase the selectivity of the sensor, nanowires should be selected which possess high catalytic activity

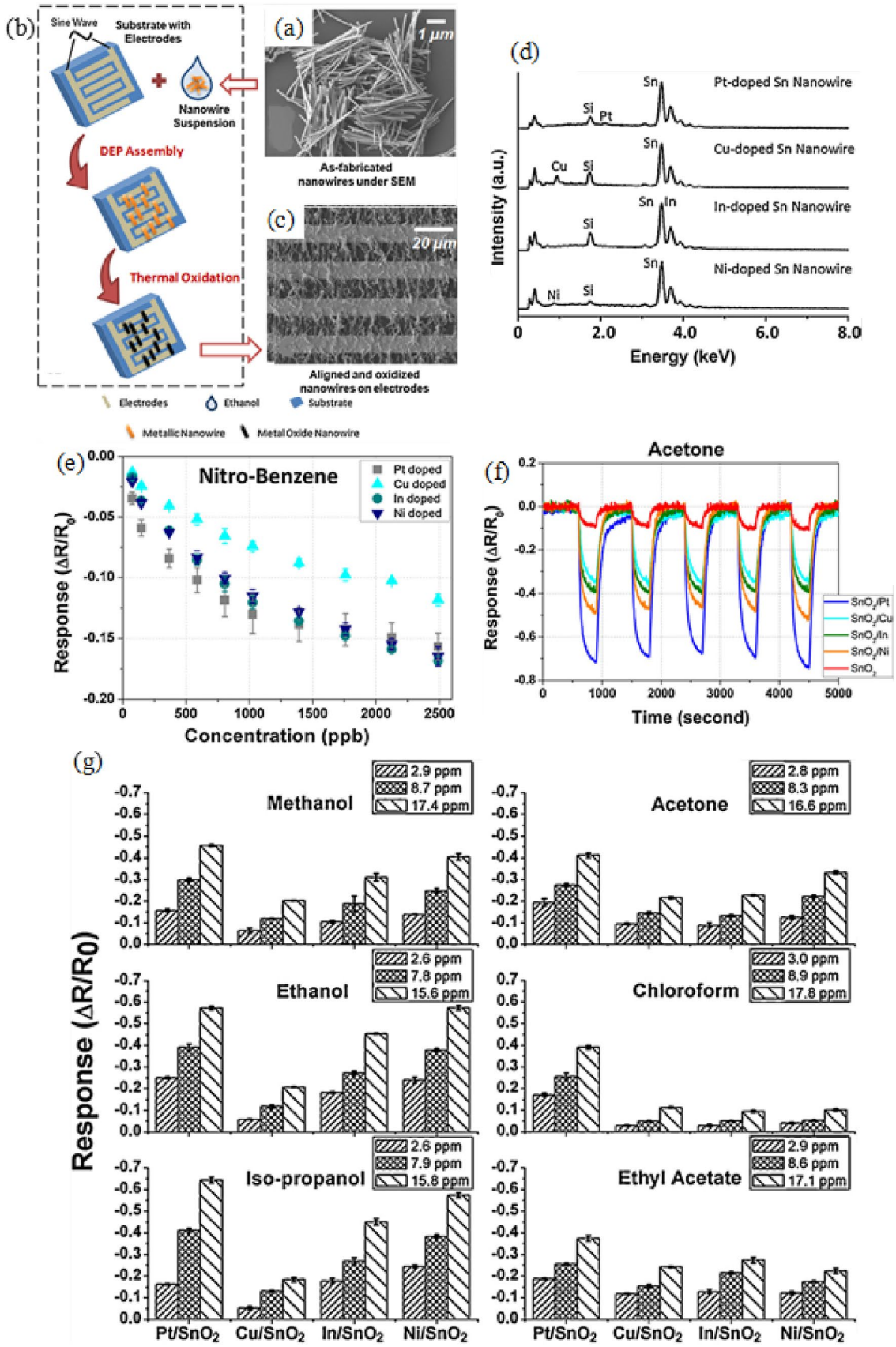
(b)
Sine Wave
Substrate with Electrodes
Nanowire Suspension
DEP Assembly
Thermal Oxidation
Electrodes
Ethanol
Substrate
Metallic Nanowire
MetalOxide Nanowire
(a)
1 μm
As-fabricated nanowires under SEM
(c)
20 μm
Aligned and oxidized nanowires on electrodes
(d)
Pt-doped Sn Nanowire
Cu-doped Sn Nanowire
In-doped Sn Nanowire
Ni-doped Sn Nanowire
Intensity (a.u.)
Energy (keV)
(e)
Nitro-Benzene
Pt doped
Cu doped
In doped
Ni doped
Response (ΔR/R0)
Concentration (ppb)
(f)
Acetone
Response (ΔR/R0)
Time (second)
SnO2/Pt
SnO2/Cu
SnO2/In
SnO2/Ni
SnO2
(g)
Methanol
2.9 ppm
8.7 ppm
17.4 ppm
Acetone
2.8 ppm
8.3 ppm
16.6 ppm
Ethanol
2.6 ppm
7.8 ppm
15.6 ppm
Chloroform
3.0 ppm
8.9 ppm
17.8 ppm
Iso-propanol
2.6 ppm
7.9 ppm
15.8 ppm
Ethyl Acetate
2.9 ppm
8.6 ppm
17.1 ppm
Response (ΔR/R0)
Pt/SnO2
Cu/SnO2
In/SnO2
Ni/SnO2

◂**Fig. 16** **a** SEM picture of as-fabricated doped tin nanowires, **b** sensor chip manufacturing schematic design; and, **c** SEM image of doped tin oxide nanowires following this process, **d** A representation of the EDS spectra of doped tin oxide nanowires (from top to bottom: Pt, Cu, In and Ni dopants), **e** Static sensor response of four doped tin oxide nanowires to nitro-benzene at ten concentration levels, **f** Five times, the sensor array's dynamic sensing tests were performed in response to acetone exposure at a concentration of 800 ppm. As a control, an undoped SnO_2 nanowire sensor was employed, **g** a bar chart depicting the response of the nanowire sensor array to volatile organic chemical vapours [78]

against the target gas, and complex structures should be designed without affecting the properties of the nanowires, such as surface area, porosity, electrical conductivity. Apart from this, though certain publications related to tin oxide nanowire as a room temperature gas sensor was found and incorporated the same. However, still there is required toproduce efficient gas sensor based on this subject to fulfil the requirement of eco-friendly gas sensing application. This may not possible because of the certain limitations of sensing property at room temperature. For instance, less number of vacancy generations of oxygen due to low temperature and atmospheric hurdle like relative humidity. This is the biggest challenge these days in the production of such a sensor that can give detection at RT, hence, researchers in the field should addressed this trouble and can prepare such a senor based on tin oxide nanowire by any possible route with required property for ideal room temperature gas sensor. In the future, scientists in this field should put more emphasis on the fabrication of these types of chemiresitive gas sensors. Finally, we believe that our findings will pave the way for additional research into greater room-temperature gas sensing of SnO_2 NWs and other sensing materials.

Acknowledgements Priyanka Joshi thanks the Brazilian research funding agency CNPq (164743/2021-9) for the financial support of this work.

Declarations

Conflict of interest Authors state that they do not have any conflict of interest.

References

1. V. Mounasamy, G.K. Mani, S. Madanagurusamy, Vanadium oxide nanostructures for chemiresistive gas and vapour sensing: a review on state of the art. Microchim. Acta **187**(4), 1–29 (2020). https://doi.org/10.1007/s00604-020-4182-2
2. N. Yamazoe, Toward innovations of gas sensor technology. Sens. Actuators B Chem. **108**(1–2), 2–14 (2005). https://doi.org/10.1016/j.snb.2004.12.075
3. N. Joshi, T. Hayasaka, Y. Liu, H. Liu, O.N. Oliveira, L. Lin, A review on chemiresistive room temperature gas sensors based on metal oxide nanostructures, graphene and 2D transition metal dichalcogenides. Microchim. Acta **185**(4), 1–16 (2018). https://doi.org/10.1007/s00604-018-2750-5
4. R. Malik, N. Joshi, V.K. Tomer, Advances in the designs and mechanisms of MoO_3 nanostructures for gas sensors: a holistic review. Mater. Adv. **2**(13), 4190–4227 (2021). https://doi.org/10.1039/D1MA00374G
5. H. Wang, W.P. Lustig, J. Li, Sensing and capture of toxic and hazardous gases and vapors by metal–organic frameworks. Chem. Soc. Rev. **47**(13), 4729–4756 (2018). https://doi.org/10.1039/C7CS00885F
6. A. Gusain, N.J. Joshi, P.V. Varde, D.K. Aswal, Flexible NO gas sensor based on conducting polymer poly [N-9′-heptadecanyl-2, 7-carbazole-alt-5, 5-(4′, 7′-di-2-thienyl-2′, 1′, 3′-benzothiadiazole)](PCDTBT). Sens. Actuators B Chem. **239**, 734–745 (2017). https://doi.org/10.1016/j.snb.2016.07.176
7. R. Malik, V.K. Tomer, N. Joshi, V. Chaudhary, L. Lin, Nanosensors for monitoring indoor pollution in smart cities, in *Nanosensors for Smart Cities*. ed. by B. Han, V.K. Tomer, T. Anh Nguyen, A. Farmani, P.K. Singh (Elsevier, Amsterdam, 2020), pp. 251–266
8. F. Mustafa, S. Andreescu, Chemical and biological sensors for food-quality monitoring and smart packaging. Foods **7**(10), 168 (2018). https://doi.org/10.3390/foods7100168
9. G. Korotcenkov, B.K. Cho, Metal oxide composites in conductometric gas sensors: achievements and challenges. Sens. Actuators B Chem. **244**, 182–210 (2017). https://doi.org/10.1016/j.snb.2016.12.117
10. Y. Kong, Y. Li, X. Cui, L. Su, D. Ma, T. Lai, L. Yao, X. Xiao, Y. Wang, SnO_2 nanostructured materials used as gas sensors for the detection of hazardous and flammable gases: a review. Nano Mater. Sci. (2021). https://doi.org/10.1016/j.nanoms.2021.05.006
11. A. Hartzell, M. da Silva, Reliability issues in miniaturized sensors: importance of standards. What is needed?. in, *2007 IEEE Sensors*, pp. 44–44 (2007). https://doi.org/10.1109/ICSENS.2007.4388331
12. S. Thomas, N. Joshi, V.K. Tomer, *Functional Nanomaterials: Advances in Gas Sensing Technologies*, 1st edn. (Springer, Singapore, 2020), p. 1
13. N. Joshi, M.L. Braunger, F.M. Shimizu, A. Riul, O.N. Oliveira, Two-dimensional transition metal dichalcogenides for gas sensing applications, in *Nanosensors for Environmental Applications*. ed. by S.K. Tuteja, D. Arora, N. Dilbaghi, E. Lichtfouse (Springer, Cham, 2020), pp. 131–155
14. A. Kar, A. Patra, Recent development of core–shell SnO_2 nanostructures and their potential applications. J. Mater. Chem. C **2**(33), 6706–6722 (2014). https://doi.org/10.1039/C4TC01030B
15. X. Pang, M.D. Shaw, S. Gillot, A.C. Lewis, The impacts of water vapour and co-pollutants on the performance of electrochemical gas sensors used for air quality monitoring. Sens. Actuators B Chem. **266**, 674–684 (2018). https://doi.org/10.1016/j.snb.2018.03.144
16. Y.F. Sun, S.B. Liu, F.L. Meng, J.Y. Liu, Z. Jin, L.T. Kong, J.H. Liu, Metal oxide nanostructures and their gas sensing properties: a review. Sensors **12**(3), 2610–2631 (2012). https://doi.org/10.3390/s120302610
17. W. Qing, L. Yong-ping, L. Wei-long, Development of a multicomponent infrared gas sensor detection system. J. Phys. Conf. Ser. **1229**(1), 012068 (2019). https://doi.org/10.1088/1742-6596/1229/1/012068
18. E.M. Materon, F.R. Gómez, N. Joshi, C.J. Dalmaschio, E. Carrilho, O.N. Oliveira Jr., Smart materials for electrochemical flexible nanosensors: advances and applications, in *Nanosensors for Smart Manufacturing*. ed. by S. Thomas, T. Anh Nguyen, M. Ahmadi, A. Farmani, G. Yasin (Elsevier, Amsterdam, 2021), pp. 347–371

19. C.M. Miyazaki, N. Joshi, O.N. Oliveira, F.M. Shimizu, Metal oxides and sulfide-based biosensors for monitoring and health control, in *Metal, Metal-Oxides and Metal Sulfides for Batteries, Fuel Cells, Solar Cells, Photocatalysis and Health Sensors*. ed. by S. Rajendran, H. Karimi-Maleh, J. Qin, E. Lichtfouse (Springer, Cham, 2021), pp. 169–208
20. E.M. Materon, A. Wong, L.M. Gomes, G. Ibanez-Redin, N. Joshi, O.N. Oliveira, R.C. Faria, Combining 3D printing and screen-printing in miniaturized, disposable sensors with carbon paste electrodes. J. Mater. Chem. C **9**(17), 5633–5642 (2021). https://doi.org/10.1039/D1TC01557E
21. E.M. Materon, N. Joshi, F.M. Shimizu, R.C. Faria, O.N. Oliveira Jr., *Electrochemical Sensors Based on Metal Oxide-Boron Nitride Nanocomposites in the Detection of Biomolecules and Toxic Chemicals, Metal Oxides in Nanocomposite-Based Electrochemical Sensors for Toxic Chemicals* (Elsevier, Amsterdam, 2021), pp. 293–311
22. M. Vasudevan, M.J. Tai, V. Perumal, S.C. Gopinath, S.S. Murthe, M. Ovinis, N.M. Mohamed, N. Joshi, Cellulose acetate-MoS_2 nanopetal hybrid: a highly sensitive and selective electrochemical aptasensor of Troponin I for the early diagnosis of acute myocardial infarction. J. Taiwan. Inst. Chem. Eng. **118**, 245–253 (2021). https://doi.org/10.1016/j.jtice.2021.01.016
23. M. Vasudevan, M.J. Tai, V. Perumal, S.C. Gopinath, S.S. Murthe, M. Ovinis, N.M. Mohamed, N. Joshi, Highly sensitive and selective acute myocardial infarction detection using aptamer-tethered MoS_2 nanoflower and screen-printed electrodes. Biotechnol. Appl. Biochem. (2020). https://doi.org/10.1002/bab.2060
24. E.M. Materon, G. Ibáñez-Redín, N. Joshi, D. Gonçalves, O.N. Oliveira, R.C. Faria, Analytical detection of pesticides, pollutants, and pharmaceutical waste in the environment, in *Nanosensors for Environmental Applications*. ed. by S.K. Tuteja, D. Arora, N. Dilbaghi, E. Lichtfouse (Springer, Cham, 2020), pp. 87–129
25. G. Ibáñez-Redín, N. Joshi, G.F. Nascimento, D. Wilson, M.E. Melendez, A.L. Carvalho, R.M. Reis, D. Gonçalves, O.N. Oliveira, Determination of p53 biomarker using an electrochemical immunoassay based on layer-by-layer films with $NiFe_2O_4$ nanoparticles. Microchim. Acta **187**(11), 1–10 (2020). https://doi.org/10.1007/s00604-020-04594-z
26. J. Hodgkinson, R.P. Tatam, Optical gas sensing: a review. Meas. Sci. Technol. **24**(1), 012004 (2012). https://doi.org/10.1088/0957-0233/24/1/012004
27. R. Malik, V.K. Tomer, V. Chaudhary, N. Joshi, S. Duhan, Semiconducting metal oxides for photocatalytic and gas sensing applications, in *Metal Oxide Nanocomposites: Synthesis and Applications*. ed. by B. Raneesh, P.M. Visakh (Wiley, Hoboken, 2020), pp. 265–301
28. N. Joshi, V.K. Tomer, R. Malik, J. Nie, Recent advances on UV-enhanced oxide nanostructures gas sensors, in *Functional Nanomaterials. Materials Horizons: From Nature to Nanomaterials*. ed. by S. Thomas, N. Joshi, V. Tomer (Springer, Singapore, 2020), pp. 142–159
29. W. Tang, J. Wang, Enhanced gas sensing mechanisms of metal oxide heterojunction gas sensors. Acta Physico-ChimicaSinica **32**(5), 1087–1104 (2016). https://doi.org/10.3866/PKU.WHXB201602224
30. A. Ponzoni, C. Baratto, N. Cattabiani, M. Falasconi, V. Galstyan, E. Nunez-Carmona, F. Rigoni, V. Sberveglieri, G. Zambotti, D. Zappa, Metal oxide gas sensors, a survey of selectivity issues addressed at the SENSOR Lab, Brescia (Italy). Sensors **17**(4), 714 (2017). https://doi.org/10.3390/s17040714
31. T. Gessner, K. Gottfried, R. Hoffmann, C. Kaufmann, U. Weiss, E. Charetdinov, P. Hauptmann, R. Lucklum, B. Zimmermann, U. Dietel, G. Springer, M. Vogel, Metal oxide gas sensor for high temperature application. Microsyst. Technol. **6**(5), 169–174 (2000). https://doi.org/10.1007/s005420000048
32. C. Wang, L. Yin, L. Zhang, D. Xiang, R. Gao, Metal oxide gas sensors: sensitivity and influencing factors. Sensors **10**(3), 2088–2106 (2010). https://doi.org/10.3390/s100302088
33. A. Arbab, A. Spetz, I. Lundström, Gas sensors for high temperature operation based on metal oxide silicon carbide (MOSiC) devices. Sens. Actuators B Chem. **15**(1–3), 19–23 (1993). https://doi.org/10.1016/0925-4005(93)85022-3
34. X. Liu, N. Chen, B. Han, X. Xiao, G. Chen, I. Djerdj, Y. Wang, Nanoparticle cluster gas sensor: Pt activated SnO_2 nanoparticles for NH_3 detection with ultrahigh sensitivity. Nanoscale **7**(36), 14872–14880 (2015). https://doi.org/10.1039/C5NR03585F
35. I. Rawal, Facial synthesis of hexagonal metal oxide nanoparticles for low temperature ammonia gas sensing applications. RSC Adv. **5**(6), 4135–4142 (2015). https://doi.org/10.1039/C4RA12747A
36. B. Wang, L.F. Zhu, Y.H. Yang, N.S. Xu, G.W. Yang, Fabrication of a SnO_2 nanowire gas sensor and sensor performance for hydrogen. J. Phys. Chem. C. **112**(17), 6643–6647 (2008). https://doi.org/10.1021/jp8003147
37. H. Huang, C.Y. Ong, J. Guo, T. White, M.S. Tse, O.K. Tan, Pt surface modification of SnO_2 nanorod arrays for CO and H_2 sensors. Nanoscale **2**(7), 1203–1207 (2010). https://doi.org/10.1039/C0NR00159G
38. W. Chen, Z. Qin, Y. Liu, Y. Zhang, Y. Li, S. Shen, Z.M. Wang, H.Z. Song, Promotion on acetone sensing of single SnO_2 nanobelt by Eu doping. Nanoscale Res. Lett. **12**(1), 1–7 (2017). https://doi.org/10.1186/s11671-017-2177-7
39. S.H. Hahn, N. Barsan, U. Weimar, S.G. Ejakov, J.H. Visser, R.E. Soltis, CO sensing with SnO_2 thick film sensors: role of oxygen and water vapour. Thin Solid Films **436**(1), 17–24 (2003). https://doi.org/10.1016/S0040-6090(03)00520-0
40. P. Stefanov, G. Atanasova, E. Manolov, Z. Raicheva, V. Lazarova, Preparation and characterization of SnO_2 films for sensing applications. J. Phys. Conf. Ser. **100**(8), 082046 (2008). https://doi.org/10.1088/1742-6596/100/8/082046
41. M. Wu, W. Zeng, Y. Li, Hydrothermal synthesis of novel SnO_2 nanoflowers and their gas-sensing properties. Mater. Lett. **104**, 34–36 (2013). https://doi.org/10.1016/j.matlet.2013.04.010
42. Y. Wang, X. Wu, Y. Li, Z. Zhou, Mesostructured SnO_2 as sensing material for gas sensors. Solid-State Electron. **48**(5), 627–632 (2004). https://doi.org/10.1016/j.sse.2003.09.015
43. E. Garnett, L. Mai, P. Yang, Introduction: 1D nanomaterials/nanowires. Chem. Rev. **119**(15), 8955–8957 (2019). https://doi.org/10.1021/acs.chemrev.9b00423
44. Z. Song, S. Xu, M. Li, W. Zhang, H. Yu, Y. Wang, H. Liu, Solution-processed SnO_2 nanowires for sensitive and fast-response H_2S detection. Thin Solid Films **618**, 232–237 (2016). https://doi.org/10.1016/j.tsf.2016.08.020
45. A. Kumar, N. Joshi, Self-powered environmental monitoring gas sensors: piezoelectric and triboelectric approaches, in *Micro and Nano Technologies Nanobatteries and Nanogenerators*. ed. by H. Song, R. Venkatachalam, T.A. Nguyen, H.B. Wu, P. Nguyen-Tri (Elsevier, Amsterdam, 2021), pp. 463–489
46. R.A. Gonçalves, R.P. Toledo, N. Joshi, O.M. Berengue, Green synthesis and applications of ZnO and TiO_2 nanostructures. Molecules **26**(8), 2236 (2021). https://doi.org/10.3390/molecules26082236
47. Z. Liu, D. Zhang, S. Han, C. Li, T. Tang, W. Jin, X. Liu, B. Lei, C. Zhou, Laser ablation synthesis and electron transport studies of tin oxide nanowires. Adv. Mater. **15**(20), 1754–1757 (2003). https://doi.org/10.1002/adma.200305439
48. G. Korotcenkov, *Tin Oxide Materials: Synthesis, Properties, and Applications*, 1st edn. (Elsevier, Amsterdam, 2020), p. 3

49. S. Das, V. Jayaraman, SnO_2: a comprehensive review on structures and gas sensors. Prog. Mater. Sci. **66**, 112–255 (2014). https://doi.org/10.1016/j.pmatsci.2014.06.003
50. L. Gracia, A. Beltrán, J. Andrés, Characterization of the high-pressure structures and phase transformations in SnO_2. A density functional theory study. J. Phys. Chem. **111**(23), 6479–6485 (2007). https://doi.org/10.1021/jp067443v
51. L.A. Errico, Ab initio FP-LAPW study of the semiconductors SnO and SnO_2. Phys. B Condens. Matter **389**(1), 140–144 (2007). https://doi.org/10.1016/j.physb.2006.07.041
52. J. Xu, S. Huang, Z. Wang, First principle study on the electronic structure of fluorine-doped SnO_2. Solid State Commun. **149**(13–14), 527–531 (2009). https://doi.org/10.1016/j.ssc.2009.01.010
53. L.I. Nadaf, K.S. Venkatesh, Synthesis and characterization of tin oxide nanoparticles by co-precipitation method. IOSR J. Appl. Chem. **9**(2), 1–4 (2016)
54. B. Wang, Y.H. Yang, C.X. Wang, G.W. Yang, Growth and photoluminescence of SnO_2 nanostructures synthesized by Au–Ag alloying catalyst assisted carbothermal evaporation. Chem. Phys. Lett. **407**(4–6), 347–353 (2005). https://doi.org/10.1016/j.cplett.2005.03.119
55. M. Batzill, U. Diebold, The surface and materials science of tin oxide. Prog. Surf. Sci. **79**(2–4), 47–154 (2005). https://doi.org/10.1016/j.progsurf.2005.09.002
56. M. Kwoka, B. Lyson-Sypien, A. Kulis, D. Zappa, E. Comini, Surface properties of SnO_2 nanowires deposited on Si substrate covered by Au catalyst studies by XPS, TDS and SEM. Nanomaterials **8**(9), 738 (2018). https://doi.org/10.3390/nano8090738
57. R.K. Joshi, A. Kumar, Room temperature gas detection using silicon nanowires. Mater. Today **14**(1–2), 52 (2011). https://doi.org/10.1016/S1369-7021(11)70034-7
58. Y. Cai, H. Fan, One-step self-assembly economical synthesis of hierarchical ZnO nanocrystals and their gas-sensing properties. Cryst. Eng. Comm. **15**(44), 9148–9153 (2013). https://doi.org/10.1039/C3CE41374H
59. J. Guo, J. Zhang, M. Zhu, D. Ju, H. Xu, B. Cao, High-performance gas sensor based on ZnO nanowires functionalized by Au nanoparticles. Sens. Actuators B Chem. **199**, 339–345 (2019). https://doi.org/10.1016/j.snb.2014.04.010
60. P. Patil, G. Gaikwad, D.R. Patil, J. Naik, Synthesis of 1-D ZnO nanorods and polypyrrole/1-D ZnO nanocomposites for photocatalysis and gas sensor applications. Bull. Mater. Sci. **39**(3), 655–665 (2016). https://doi.org/10.1007/s12034-016-1208-9
61. L. Zhu, W. Zeng, Room-temperature gas sensing of ZnO-based gas sensor: a review. Sens. Actuator A Phys. **267**, 242–261 (2017). https://doi.org/10.1016/j.sna.2017.10.021
62. Z.S. Hosseini, A. Mortezaali, Room temperature H_2S gas sensor based on rather aligned ZnO nanorods with flower-like structures. Sens. Actuators B Chem. **207**, 865–871 (2015). https://doi.org/10.1016/j.snb.2014.10.085
63. G. Korotcenkov, B.K. Cho, The role of grain size on the thermal instability of nanostructured metal oxides used in gas sensor applications and approaches for grain-size stabilization. Prog. Cryst. Growth Charact Mater. **58**(4), 167–208 (2012). https://doi.org/10.1016/j.pcrysgrow.2012.07.001
64. D. Zhang, C. Jiang, Y. Yao, D. Wang, Y. Zhang, Room-temperature highly sensitive CO gas sensor based on Ag-loaded zinc oxide/molybdenum disulfide ternary nanocomposite and its sensing properties. Sens. Actuators B Chem. **253**, 1120–1128 (2017). https://doi.org/10.1016/j.snb.2017.07.173
65. X. Geng, C. Zhang, M. Debliquy, Cadmium sulfide activated zinc oxide coatings deposited by liquid plasma spray for room temperature nitrogen dioxide detection under visible light illumination. Ceram. Int. **42**(4), 4845–4852 (2016). https://doi.org/10.1016/j.ceramint.2015.11.170
66. Y. Wu, N. Joshi, S. Zhao, H. Long, L. Zhou, G. Ma, B. Peng, O.N. Oliveira Jr., A. Zettl, L. Lin, NO_2 gas sensors based on CVD tungsten diselenide monolayer. Appl. Surf. Sci. **529**, 147110 (2020). https://doi.org/10.1016/j.apsusc.2020.147110
67. P.K. Mishra, R. Malik, V.K. Tomer, N. Joshi, Hybridized graphitic carbon nitride (g-CN) as high performance VOCs sensor, in *Functional Nanomaterials*. ed. by S. Thomas, N. Joshi, V. Tomer (Springer, Singapore, 2020), pp. 285–302
68. E.M. Materón, C.M. Miyazaki, O. Carr, N. Joshi, P.H. Picciani, C.J. Dalmaschio, F. Davis, F.M. Shimizu, Magnetic nanoparticles in biomedical applications: a review. Appl. Surf. Sci. Adv. **6**, 100163 (2021). https://doi.org/10.1016/j.apsadv.2021.100163
69. S.W. Fan, A.K. Srivastava, V.P. Dravid, UV-activated room-temperature gas sensing mechanism of polycrystalline ZnO. Appl. Surf. Sci. **95**(14), 142106 (2009). https://doi.org/10.1063/1.3243458
70. S. Mishra, C. Ghanshyam, N. Ram, R.P. Bajpai, R.K. Bedi, Detection mechanism of metal oxide gas sensor under UV radiation. Sens. Actuators B Chem. **97**(2–3), 387–390 (2004). https://doi.org/10.1016/j.snb.2003.09.017
71. P. Sundara Venkatesh, P. Dharmaraj, V. Purushothaman, V. Ramakrishnan, K. Jeganathan, Point defects assisted NH_3 gas sensing properties in ZnO nanostructures. Sens. Actuators B: Chem. **212**, 10–17 (2015). https://doi.org/10.1016/j.snb.2015.01.070
72. P. Shankar, J.B.B. Rayappan, Racetrack effect on the dissimilar sensing response of ZnO thin film-an anisotropy of isotropy. ACS Appl. Mater. Interfaces **8**(37), 24924–24932 (2016). https://doi.org/10.1021/acsami.6b05133
73. G.K. Mani, J.B.B. Rayappan, A highly selective and wide range ammonia sensor—Nanostructured ZnO: Co thin film. Mater. Sci. Eng. B **191**, 41–50 (2015). https://doi.org/10.1016/j.mseb.2014.10.007
74. G.M. Patel, V.R. Shah, G.J. Bhatt, P.T. Deota, Humidity nanosensors for smart manufacturing, in *Nanosensors for Smart Manufacturing*. ed. by S. Thomas, T.A. Nguyen, M. Ahmadi, A. Farmani, G. Yasin (Elsevier, Amsterdam, 2021), pp. 555–580
75. J. Nie, Y. Wu, Q. Huang, N. Joshi, N. Li, X. Meng, S. Zheng, M. Zhang, B. Mi, L. Lin, Dew point measurement using a carbon-based capacitive sensor with active temperature control. ACS Appl. Mater. Interfaces **11**(1), 1699–1705 (2018). https://doi.org/10.1021/acsami.8b18538
76. Y. Wu, Q. Huang, J. Nie, J. Liang, N. Joshi, T. Hayasaka, S. Zhao, M. Zhang, X. Wang, L. Lin, All-carbon based flexible humidity sensor. J. Nanosci. Nanotechnol. **19**(8), 5310–5316 (2019). https://doi.org/10.1166/jnn.2019.16821
77. N. Ramgir, N. Datta, M. Kaur, S. Kailasaganapathi, A.K. Debnath, D.K. Aswal, S.K. Gupta, Metal oxide nanowires for chemiresistive gas sensors: issues, challenges and prospects. Colloids Surf. A Physicochem. Eng. Asp. **439**, 101–116 (2013). https://doi.org/10.1016/j.colsurfa.2013.02.029
78. X. Li, J.H. Cho, P. Kurup, Z. Gu, Novel sensor array based on doped tin oxide nanowires for organic vapor detection. Sens. Actuators B Chem. **162**(1), 251–258 (2012). https://doi.org/10.1016/j.snb.2011.12.075
79. J.P. Cheng, J. Wang, Q.Q. Li, H.G. Liu, Y. Li, A review of recent developments in tin dioxide composites for gas sensing application. J. Ind. Eng. Chem. **44**, 1–22 (2016). https://doi.org/10.1016/j.jiec.2016.08.008
80. D.R. Miller, S.A. Akbar, P.A. Morris, Nanoscale metal oxide-based heterojunctions for gas sensing: a review. Sens. Actuators B Chem. **204**, 250–272 (2014). https://doi.org/10.1016/j.snb.2014.07.074
81. A.A. Baharuddin, B.C. Ang, A.S.M.A. Haseeb, Y.C. Wong, Y.H. Wong, Advances in chemiresistive sensors for acetone gas

detection. Mater. Sci. Semicond. Process **103**, 104616 (2019). https://doi.org/10.1016/j.mssp.2019.104616
82. F. Xu, H.P. Ho, Light-activated metal oxide gas sensors: a review. Micromachines **8**(11), 333 (2017). https://doi.org/10.3390/mi8110333
83. N. Joshi, L.F. da Silva, F.M. Shimizu, V.R. Mastelaro, J.C. M'Peko, L. Lin, O.N. Oliveira, UV-assisted chemiresistors made with gold-modified ZnO nanorods to detect ozone gas at room temperature. Microchim. Acta **186**(7), 1–9 (2019). https://doi.org/10.1007/s00604-019-3532-4
84. R. Malik, V.K. Tomer, N. Joshi, T. Dankwort, L. Lin, L. Kienle, Au–TiO_2-loaded cubic g-C_3N_4 nanohybrids for photocatalytic and volatile organic amine sensing applications. ACS Appl. Mater. Interfaces **10**(40), 34087–34097 (2018). https://doi.org/10.1021/acsami.8b08091
85. Y. Li, D. Deng, N. Chen, X. Xing, X. Liu, X. Xiao, Y. Wang, Pd nanoparticles composited SnO_2 microspheres as sensing materials for gas sensors with enhanced hydrogen response performances. J. Alloys Compd. **710**, 216–224 (2017). https://doi.org/10.1016/j.jallcom.2017.03.274
86. Q. Ren, Y.Q. Cao, D. Arulraj, C. Liu, D. Wu, W.M. Li, A.D. Li, Resistive-type hydrogen sensors based on zinc oxide nanostructures. J. Electrochem. Soc. **167**(6), 067528 (2020). https://doi.org/10.1149/1945-7111/ab7e23
87. N. Joshi, L.F. da Silva, H. Jadhav, J.C. M'Peko, B.B.M. Torres, K. Aguir, V.R. Mastelaro, O.N. Oliveira, One-step approach for preparing ozone gas sensors based on hierarchical $NiCo_2O_4$ structures. RSC Adv. **6**(95), 92655–92662 (2016). https://doi.org/10.1039/C6RA18384K
88. N. Joshi, L.F. da Silva, H.S. Jadhav, F.M. Shimizu, P.H. Suman, J.C. M'Peko, M.O. Orlandi, J.G. Seo, V.R. Mastelaro, O.N. Oliveira Jr., Yolk-shelled $ZnCo_2O_4$ microspheres: surface properties and gas sensing application. Sens. Actuators B Chem. **257**, 906–915 (2018). https://doi.org/10.1016/j.snb.2017.11.041
89. N. Joshi, F.M. Shimizu, I.T. Awan, J.C. M'Peko, V.R. Mastelaro, O.N. Oliveira, L.F. da Silva, Ozone sensing properties of nickel phthalocyanine: ZnO nanorod heterostructures, in *2016 IEEE Sensors* pp. 1–3 (2016).: https://doi.org/10.1109/ICSENS.2016.7808407
90. Z. Wang, L. Zhu, S. Sun, J. Wang, W. Yan, One-dimensional nanomaterials in resistive gas sensor: from material design to application. Chemosensors **9**(8), 198 (2021). https://doi.org/10.3390/chemosensors9080198
91. N.J. Joshi, M.L. Braunger, F.M. Shimizu, A. Riul Jr., O.N. de Oliveira Jr, Insights into nano-heterostructured materials for gas sensing: a review. Multifunct. Mater. **4**(3), 032002 (2021). https://doi.org/10.1088/2399-7532/ac1732
92. A. Kumar, N. Joshi, S. Samanta, A. Singh, A.K. Debnath, A.K. Chauhan, S.K. Gupta, Room temperature detection of H_2S by flexible gold–cobalt phthalocyanine heterojunction thin films. Sens. Actuators B Chem. **206**, 653–662 (2015). https://doi.org/10.1016/j.snb.2014.09.074
93. P. Karnati, S. Akbar, P.A. Morris, Conduction mechanisms in one dimensional core-shell nanostructures for gas sensing: a review. Sens. Actuators B Chem. **295**, 127–143 (2019). https://doi.org/10.1016/j.snb.2019.05.049
94. H. Ogawa, M. Nishikawa, A. Abe, Hall measurement studies and an electrical conduction model of tin oxide ultrafine particle films. J. Appl. Phys. **53**(6), 4448–4455 (1982). https://doi.org/10.1063/1.331230
95. S.M. Sze, Y. Li, K.K. Ng, *Physics of Semiconductor Devices*, 4th edn. (Wiley, Hoboken, 2021), p. 835
96. M.E. Franke, T.J. Koplin, U. Simon, Metal and metal oxide nanoparticles in chemiresistors: does the nanoscale matter? Small **2**(1), 36–50 (2006). https://doi.org/10.1002/smll.200500261
97. V.K. Tomer, R. Malik, N. Joshi, A special section on applications of 2D/3D materials in sensing and photocatalysis. J. Nanosci. Nanotechnol. **19**(8), 5052–5053 (2019). https://doi.org/10.1166/jnn.2019.16841
98. A. Mekki, N. Joshi, A. Singh, Z. Salmi, P. Jha, P. Decorse, S. Lau-Truong, R. Mahmoud, M.M. Chehimi, D.K. Aswal, S.K. Gupta, H_2S sensing using in situ photo-polymerized polyaniline–silver nanocomposite films on flexible substrates. Org. Electron. **15**(1), 71–81 (2014). https://doi.org/10.1016/j.orgel.2013.10.012
99. A. Singh, A. Kumar, A. Kumar, S. Samanta, N. Joshi, V. Balouria, A.K. Debnath, R. Prasad, Z. Salmi, M.M. Chehimi, D.K. Aswal, Bending stress induced improved chemiresistive gas sensing characteristics of flexible cobalt-phthalocyanine thin films. Appl. Phys. Lett. **102**(13), 132107 (2013). https://doi.org/10.1063/1.4800446
100. K. Wetchakun, T. Samerjai, N. Tamaekong, C. Liewhiran, C. Siriwong, V. Kruefu, A. Wisitsoraat, A. Tuantranont, S. Phanichphant, Semiconducting metal oxides as sensors for environmentally hazardous gases. Sens. Actuators B Chem. **160**(1), 580–591 (2011). https://doi.org/10.1016/j.snb.2011.08.032
101. S.J. Patil, A.V. Patil, C.G. Dighavkar, K.S. Thakare, R.Y. Borase, S.J. Nandre, N.G. Deshpande, R.R. Ahire, Semiconductor metal oxide compounds based gas sensors: a literature review. Front. Mater. Sci. **9**(1), 14–37 (2015). https://doi.org/10.1007/s11706-015-0279-7
102. A. Mirzaei, J.H. Lee, S.M. Majhi, M. Weber, M. Bechelany, H.W. Kim, S.S. Kim, Resistive gas sensors based on metal-oxide nanowires. J. Appl. Phys. **126**(24), 241102 (2019). https://doi.org/10.1063/1.5118805
103. A. Gurlo, N. Bârsan, U. Weimar, Gas sensors based on semiconducting metal oxides, in *Metal Oxides: Chemistry and Applications*. ed. by J.L.G. Fierro (CRC Press, Boca Raton, 2005), pp. 683–738
104. A.T. Güntner, N.J. Pineau, P. Mochalski, H. Wiesenhofer, A. Agapiou, C.A. Mayhew, S.E. Pratsinis, Sniffing entrapped humans with sensor arrays. Anal. Chem. **90**(8), 4940–4945 (2018). https://doi.org/10.1021/acs.analchem.8b00237
105. D. Wei, W. Jiang, H. Gao, X. Chuai, F. Liu, F. Liu, P. Sun, X. Liang, Y. Gao, X. Yan, G. Lu, Facile synthesis of La-doped In2O3 hollow microspheres and enhanced hydrogen sulfide sensing characteristics. Sens. Actuators B Chem. **276**, 413–420 (2018). https://doi.org/10.1016/j.snb.2018.08.130
106. Y. Xu, L. Zheng, C. Yang, X. Liu, J. Zhang, Highly sensitive and selective electronic sensor based on Co catalyzed SnO_2 nanospheres for acetone detection. Sens. Actuators B Chem. **304**, 127237 (2020). https://doi.org/10.1016/j.snb.2019.127237
107. O. Lupan, L. Chow, G. Chai, A. Schulte, S. Park, H. Heinrich, A rapid hydrothermal synthesis of rutile SnO_2 nanowires. Mater. Sci. Eng. B **157**(1–3), 101–104 (2009). https://doi.org/10.1016/j.mseb.2008.12.035
108. R.A.B. John, A.R. Kumar, A review on resistive-based gas sensors for the detection of volatile organic compounds using metal-oxide nanostructures. Inorg. Chem. Commun. **13**, 108893 (2021). https://doi.org/10.1016/j.inoche.2021.108893
109. S. Sagadevan, M. Johan, R. Bin, F.A. Aziz, H.L. Hsu, R. Selvin, H.H. Hegazy, A. Umar, H. Algarni, S.L. Roselin, Influence of Mn Doping on the properties of tin oxide nanoparticles prepared by co-precipitation method. J. Nanoelectron. Optoelectron. **14**(4), 583–592 (2019). https://doi.org/10.1166/jno.2019.2588
110. D. Yu, D. Wang, W. Yu, Y. Qian, Synthesis of ITO nanowires and nanorods with corundum structure by a co-precipitation-anneal method. Mater. Lett. **58**(1–2), 84–87 (2004). https://doi.org/10.1016/S0167-577X(03)00420-8
111. Y.X. Gan, A.H. Jayatissa, Z. Yu, X. Chen, M. Li, Hydrothermal synthesis of nanomaterials. J. Nanomater. **2020**, 1–3 (2020). https://doi.org/10.1155/2020/8917013

112. M. Shandilya, R. Rai, J. Singh, Hydrothermal technology for smart materials. Adv. Appl. Ceram. **115**(6), 354–376 (2016). https://doi.org/10.1080/17436753.2016.1157131
113. H. Ghobarkar, O. Schäf, U. Guth, The use of the high pressure hydrothermal method for tailored synthesis of zeolites without structure directing agents. Instance: synthesis of natural zeolites with 5–1 building units. Int. J. High Pressure Res. **20**(1–6), 45–53 (2001). https://doi.org/10.1080/08957950108206151
114. O. Schäf, H. Ghobarkar, P. Knauth, Hydrothermal synthesis of nanomaterials, in *Nanostructured Materials. Electronic Materials: Science & Technology*. ed. by P. Knauth, J. Schoonman (Springer, Boston, 2004), pp. 23–41
115. M.S. Whittingham, J.D. Guo, R. Chen, T. Chirayil, G. Janauer, P. Zavalij, The hydrothermal synthesis of new oxide materials. Solid State Ion. **75**, 257–268 (1995). https://doi.org/10.1016/0167-2738(94)00220-M
116. S. Gupta, M. Tripathi, A review on the synthesis of TiO_2 nanoparticles by solution route. Open Chem. **10**(2), 279–294 (2012). https://doi.org/10.2478/s11532-011-0155-y
117. M. Parashar, V.K. Shukla, R. Singh, Metal oxides nanoparticles via sol–gel method: a review on synthesis, characterization and applications. J. Mater. Sci. Mater. Electron. **31**(5), 3729–3749 (2020). https://doi.org/10.1007/s10854-020-02994-8
118. G.J. Owens, R.K. Singh, F. Foroutan, M. Alqaysi, C.M. Han, C. Mahapatra, H.W. Kim, J.C. Knowles, Sol–gel based materials for biomedical applications. Prog. Mater. Sci. **77**, 1–79 (2016). https://doi.org/10.1016/j.pmatsci.2015.12.001
119. A.V. Rane, K. Kanny, V.K. Abitha, S. Thomas, Methods for synthesis of nanoparticles and fabrication of nanocomposites, in *Synthesis of Inorganic Nanomaterials*. ed. by S.M. Bhagyaraj, O.S. Oluwafemi, N.K. Kalarikkal, S. Thomas (Woodhead Publishing, Sawston, 2018), pp. 121–139
120. H.W. Wang, C.F. Ting, M.K. Hung, C.H. Chiou, Y.L. Liu, Z. Liu, K.R. Ratinac, S.P. Ringer, Three-dimensional electrodes for dye-sensitized solar cells: synthesis of indium–tin-oxide nanowire arrays and ITO/TiO_2 core–shell nanowire arrays by electrophoretic deposition. Nanotechnology **20**(5), 055601 (2009). https://doi.org/10.1088/0957-4484/20/5/055601
121. X. Shi, W. Zhou, D. Ma, Q. Ma, D. Bridges, Y. Ma, A. Hu, Electrospinning of nanofibers and their applications for energy devices. J. Nanomater. **16**(1), 122 (2015). https://doi.org/10.1155/2015/140716
122. J. Wu, J.L. Coffer, Strongly emissive erbium-doped tin oxide nanofibers derived from sol gel/electrospinning methods. J. Phys. Chem. C **111**(44), 16088–16091 (2007). https://doi.org/10.1021/jp076338y
123. P.S. Archana, R. Jose, C. Vijila, S. Ramakrishna, Improved electron diffusion coefficient in electrospun TiO2 nanowires. J. Phys. Chem. C **113**(52), 21538–21542 (2009). https://doi.org/10.1021/jp908238q
124. Y. Feng, W. Hou, X. Zhang, P. Lv, Y. Li, W. Feng, Highly sensitive reversible light-driven switches using electrospun porous aluminum-doped zinc oxide nanofibers. J. Phys. Chem. C **115**(10), 3956–3961 (2011). https://doi.org/10.1021/jp1117745
125. H.S. Shim, J.W. Kim, Y.E. Sung, W.B. Kim, Electrochromic properties of tungsten oxide nanowires fabricated by electrospinning method. Sol. Energy Mater. Sol. Cells **93**(12), 2062–2068 (2009). https://doi.org/10.1016/j.solmat.2009.02.008
126. R. Li, S. Chen, Z. Lou, L. Li, T. Huang, Y. Song, D. Chen, G. Shen, Fabrication of porous SnO_2 nanowires gas sensors with enhanced sensitivity. Sens. Actuators B Chem. **252**, 79–85 (2017). https://doi.org/10.1016/j.snb.2017.05.161
127. S. Coskun, B. Aksoy, H.E. Unalan, Polyol synthesis of silver nanowires: an extensive parametric study. Cryst. Growth Des. **11**(11), 4963–4969 (2011). https://doi.org/10.1021/cg200874g
128. K.S. Shankar, A.K. Raychaudhuri, Fabrication of nanowires of multicomponent oxides: review of recent advances. Mater. Sci. Eng. C **25**(5–8), 738–751 (2005). https://doi.org/10.1016/j.msec.2005.06.054
129. F. Fiévet, R. Brayner, The polyol process, in *Nanomaterials: A Danger or a Promise?*. ed. by R. Brayner, F. Fiévet, T. Coradin (Springer, London, 2013), pp. 1–25
130. X. Jiang, Y. Wang, T. Herricks, Y. Xia, Ethylene glycol-mediated synthesis of metal oxide nanowires. J. Mater. Chem. **14**(4), 695–703 (2004). https://doi.org/10.1039/B313938G
131. Y.M. Manawi, A. Samara, T. Al-Ansari, M.A. Atieh, A review of carbon nanomaterials' synthesis via the chemical vapor deposition (CVD) method. Materials **11**(5), 822 (2015). https://doi.org/10.3390/ma11050822
132. P.M. Martin, *Handbook of Deposition Technologies for Films and Coatings: Science, Applications and Technology*, 3rd edn. (Elsevier, Amsterdam, 2009), p. 314
133. J.H. Park, T.S. Sudarshan, *Chemical Vapor Deposition*, 2nd edn. (ASM International, Materials Park, 2001), p. 1
134. S. Kleckley, H. Wang, I. Oladeji, L. Chow, T.K. Daly, P.R. Buseck, T. Solouki, A. Marshall, Fullerenes and polymers produced by the chemical vapor deposition method, in *Synthesis and Characterization of Advanced Materials*. ed. by M.A. Serio, D.M. Gruen, R. Malhotra (ACS Publication, Washington DC, 1998), pp. 51–60
135. W. Jeong, H.C. Kang, Thermal chemical vapor deposition of tin oxide nanowires in a hydrogen reduction atmosphere. Ceram. Int. **44**(8), 9801–9808 (2018). https://doi.org/10.1016/j.ceramint.2018.02.217
136. R. Ilangovan, V. Subha, R.E. Ravindran, S. Kirubanandan, S. Renganathan, *Nanomaterials: Synthesis, Physicochemical Characterization, and Biopharmaceutical Applications* (Elsevier, Amsterdam, 2021), pp. 33–70
137. L. Xia, Importance of nanostructured surfaces, in *Bioceramics*. ed. by A. Osaka, R. Narayan (Elsevier, Amsterdam, 2021), pp. 5–24
138. M.S. Rafique, M. Rafique, M.B. Tahir, S. Hajra, T. Nawaz, F. Shafiq, Synthesis methods of nanostructures, in *Nanotechnology and Photocatalysis for Environmental Applications*. ed. by M.B. Tahir, M. Rafique, M.S. Rafique (Elsevier, Amsterdam, 2020), pp. 45–56
139. E. Bahadori, G. Ramis, I. Rossetti, Matching nanotechnologies with reactor scale-up and industrial exploitation, in *Nanomaterials for the Detection and Removal of Wastewater Pollutants*. ed. by B. Bonelli, F.S. Freyria, I. Rossetti, R. Sethi (Elsevier, Amsterdam, 2020), pp. 407–442
140. O. Sisman, N. Kaur, G. Sberveglieri, E. Núñez-Carmona, V. Sberveglieri, E. Comini, UV-enhanced humidity sensing of chitosan–SnO_2 hybrid nanowires. Nanomaterials **10**(2), 329 (2020). https://doi.org/10.3390/nano10020329
141. U.S. Mohanty, Electrodeposition: a versatile and inexpensive tool for the synthesis of nanoparticles, nanorods, nanowires, and nanoclusters of metals. J. Appl. Electrochem. **41**(3), 257–270 (2011). https://doi.org/10.1007/s10800-010-0234-3
142. L. Santos, J.P. Neto, A. Crespo, P. Baião, P. Barquinha, L. Pereira, R. Martins, E. Fortunato, Electrodeposition of WO_3 nanoparticles for sensing applications, in *Electroplating of Nanostructures*. ed. by M. Aliofkhazraei (IntechOpen, Vienna, 2015), pp. 1–22
143. A. Karatutlu, A. Barhoum, A. Sapelkin, Liquid-phase synthesis of nanoparticles and nanostructured materials, in *Emerging Applications of Nanoparticles and Architecture Nanostructures*. ed. by A. Barhoum, A.S. Hamdy Makhlouf (Elsevier, Amsterdam, 2018), pp. 1–28
144. A. Sharma, A. Khosla, S. Arya, Synthesis of SnO_2 nanowires as a reusable and flexible electrode for electrochemical detection of

riboflavin. Microchem. J. **156**, 104858 (2020). https://doi.org/10.1016/j.microc.2020.104858
145. M.S. Choi, H.G. Na, J.H. Bang, A. Mirzaei, S. Han, H.Y. Lee, S.S. Kim, H.W. Kim, C. Jin, SnO_2 nanowires decorated by insulating amorphous carbon layers for improved room-temperature NO_2 sensing. Sens. Actuators B Chem. **326**, 128801 (2021). https://doi.org/10.1016/j.snb.2020.128801
146. S. Park, S. An, Y. Mun, C. Lee, UV-enhanced NO_2 gas sensing properties of SnO_2-core/ZnO-shell nanowires at room temperature. ACS Appl. Mater. Interfaces **5**(10), 4285–4292 (2013). https://doi.org/10.1021/am400500a
147. J.D. Prades, R. Jiménez-Díaz, F. Hernandez-Ramirez, S. Barth, A. Cirera, A. Romano-Rodriguez, S. Mathur, J.R. Morante, Equivalence between thermal and room temperature UV light-modulated responses of gas sensors based on individual SnO_2 nanowires. Sens. Actuators B Chem. **140**(2), 337–341 (2009). https://doi.org/10.1016/j.snb.2009.04.070
148. Y.J. Kwon, S.Y. Kang, P. Wu, Y. Peng, S.S. Kim, H.W. Kim, Selective improvement of NO_2 gas sensing behavior in SnO_2 nanowires by ion-beam irradiation. ACS Appl. Mater. Interfaces **8**(21), 13646–13658 (2016). https://doi.org/10.1021/acsami.6b01619
149. J.H. Park, M.S. Cho, D. Lim, J.G. Park, SnO_2 nanowire gas sensor operating at room temperature. J. Nanosci. Nanotechnol. **14**(10), 8038–8042 (2014). https://doi.org/10.1166/jnn.2014.9403
150. N.S. Ramgir, I.S. Mulla, K.P. Vijayamohanan, A room temperature nitric oxide sensor actualized from Ru-doped SnO_2 nanowires. Sens. Actuators B Chem. **107**(2), 708–715 (2005). https://doi.org/10.1016/j.snb.2004.12.073
151. N. Ramgir, S. Sen, M. Kaur, S.K. Mishra, V. Rikka, R. Choukikar, K. Muthe, Investigation of SnO_2 nanowire based gas sensors. Asian J. Phys. **19**, 273–278 (2010)
152. Z. Song, Z. Wei, B. Wang, Z. Luo, S. Xu, W. Zhang, H. Yu, M. Li, Z. Huang, J. Zang, H. Liu, Sensitive room-temperature H_2S gas sensors employing SnO_2 quantum wire/reduced graphene oxide nanocomposites. Chem. Mater. **28**(4), 1205–1212 (2016). https://doi.org/10.1021/acs.chemmater.5b04850
153. T. Van Dang, N. Duc-Hoa, N. Van Duy, N. Van Hieu, Chlorine gas sensing performance of on-chip grown ZnO, WO_3, and SnO_2 nanowire sensors. ACS Appl. Mater. Interfaces **8**(7), 4828–4837 (2016). https://doi.org/10.1021/acsami.5b08638
154. S. Sen, P. Kanitkar, A. Sharma, K.P. Muthe, A. Rath, S.K. Deshpande, J.V. Yakhmi, Growth of $SnO_2/W_{18}O_{49}$ nanowire hierarchical heterostructure and their application as chemical sensor. Sens. Actuators B Chem. **147**(2), 453–460 (2010). https://doi.org/10.1016/j.snb.2010.04.016
155. Y. Wang, X. Jiang, Y. Xia, A solution-phase, precursor route to polycrystalline SnO_2 nanowires that can be used for gas sensing under ambient conditions. J. Am. Chem. Soc. **125**(52), 16176–16177 (2003). https://doi.org/10.1021/ja037743f
156. E.P. Stuckert, C.J. Miller, E.R. Fisher, The effect of Ar/O_2 and H_2O plasma treatment of SnO_2 nanoparticles and nanowires on carbon monoxide and benzene detection. ACS Appl. Mater. Interfaces **9**(18), 15733–15743 (2017). https://doi.org/10.1016/j.snb.2014.11.049
157. Y. Shen, T. Yamazaki, Z. Liu, D. Meng, T. Kikuta, N. Nakatani, M. Saito, M. Mori, Microstructure and H_2 gas sensing properties of undoped and Pd-doped SnO_2 nanowires. Sens. Actuators B Chem. **135**(2), 524–529 (2009). https://doi.org/10.1016/j.snb.2008.09.010
158. Y. Shen, D. Wei, M. Li, W. Liu, S. Gao, C. Han, B. Cui, Microstructure and room-temperature H_2 sensing properties of undoped and impurity-doped SnO_2 nanowires. Chem. Lett. **42**(5), 492–494 (2013). https://doi.org/10.1246/cl.130026
159. S. Deshpande, A. Karakoti, G. Londe, H.J. Cho, S. Seal, Room temperature hydrogen detection using 1-D nanostructured tin oxide sensor. J. Nanosci. Nanotechnol. **7**(9), 3354–3357 (2007). https://doi.org/10.1166/jnn.2007.872
160. Y.J. Choi, I.S. Hwang, J.G. Park, K.J. Choi, J.H. Park, J.H. Lee, Novel fabrication of an SnO_2 nanowire gas sensor with high sensitivity. Nanotechnology **19**(9), 095508 (2008). https://doi.org/10.1088/0957-4484/19/9/095508
161. M. Tonezzer, N.V. Hieu, Size-dependent response of single-nanowire gas sensors. Sens. Actuators B Chem. **163**(1), 146–152 (2012). https://doi.org/10.1016/j.snb.2012.01.022
162. E. Brunet, T. Maier, G.C. Mutinati, S. Steinhauer, A. Köck, C. Gspan, W. Grogger, Comparison of the gas sensing performance of SnO_2 thin film and SnO_2 nanowire sensors. Sens. Actuators B Chem. **165**(1), 110–118 (2012). https://doi.org/10.1016/j.snb.2012.02.025
163. H.S. Hong, T. Dai-Lam, T. Trung, N. Van Hieu, Selective detection of carbon dioxide using LaOCl-functionalized SnO2 nanowires for air-quality monitoring. Talanta **88**, 152–159 (2012). https://doi.org/10.1016/j.talanta.2011.10.024
164. X. Zhong, Y. Shen, S. Zhao, X. Chen, C. Han, D. Wei, P. Fang, D. Meng, SO_2 sensing properties of SnO_2 nanowires grown on a novel diatomite-based porous substrate. Ceram. Int. **45**(2), 2556–2565 (2019). https://doi.org/10.1016/j.ceramint.2018.10.186
165. G. Sberveglieri, C. Baratto, E. Comini, G. Faglia, M. Ferroni, A. Ponzoni, A. Vomiero, Synthesis and characterization of semiconducting nanowires for gas sensing. Sens. Actuators B Chem. **121**(1), 208–213 (2007). https://doi.org/10.1016/j.snb.2006.09.049
166. I.S. Hwang, J.K. Choi, S.J. Kim, K.Y. Dong, J.H. Kwon, B.K. Ju, J.H. Lee, Enhanced H_2S sensing characteristics of SnO_2 nanowires functionalized with CuO. Sens. Actuators B Chem. **142**(1), 105–110 (2009). https://doi.org/10.1016/j.snb.2009.07.052
167. N. Van Hieu, Comparative study of gas sensor performance of SnO_2 nanowires and their hierarchical nanostructures. Sens. Actuators B Chem. **150**(1), 112–119 (2010). https://doi.org/10.1016/j.snb.2010.07.033
168. D.C. Meier, S. Semancik, B. Button, E. Strelcov, A. Kolmakov, Coupling nanowire chemiresistors with MEMS microhotplate gas sensing platforms. Appl. Phys. Lett. **91**(6), 063118 (2007). https://doi.org/10.1063/1.2768861
169. Z. Yuan, J. Zhang, F. Meng, Y. Li, R. Li, Y. Chang, J. Zhao, E. Han, S. Wang, Highly sensitive ammonia sensors based on Ag-decorated WO_3 nanorods. IEEE Trans. Nanotechnol. **17**(6), 1252–1258 (2018). https://doi.org/10.1109/TNANO.2018.2871675
170. N.D. Hoa, P. Van Tong, N. Van Duy, T.D. Dao, H.V. Chung, T. Nagao, N. Van Hieu, Effective decoration of Pd nanoparticles on the surface of SnO_2 nanowires for enhancement of CO gas-sensing performance. J. Hazard. Mater. **265**, 124–132 (2014). https://doi.org/10.1016/j.jhazmat.2013.11.054
171. K. Shehzad, N.A. Shah, M. Amin, M. Abbas, W.A. Syed, Synthesis of SnO_2 nanowires forCO, CH_4 and CH_3OH gases sensing. Int. J. Distrib. Sens. Netw. **14**(8), 1550147718790750 (2018). https://doi.org/10.1177/2F1550147718790750
172. N. Van Duy, N.D. Hoa, N. Van Hieu, Effective hydrogen gas nanosensor based on bead-like nanowires of platinum-decorated tin oxide. Sens. Actuators B Chem. **173**, 211–217 (2012). https://doi.org/10.1016/j.snb.2012.06.079
173. A. Johari, V. Rana, M.C. Bhatnagar, Synthesis, characterization and ethanol sensing properties of tin oxide nanostructures. Nanomater. Nanotechnol. **1**, 18 (2011). https://doi.org/10.5772/2F50960

174. X.Y. Xue, Y.J. Chen, Y.G. Liu, S.L. Shi, Y.G. Wang, T.H. Wang, Synthesis and ethanol sensing properties of indium-doped tin oxide nanowires. Appl. Phys. Lett. **88**(20), 201907 (2006). https://doi.org/10.1063/1.2203941
175. I. Castro-Hurtado, J. Herrán, G.G. Mandayo, E. Castaño, SnO_2-nanowires grown by catalytic oxidation of tin sputtered thin films for formaldehyde detection. Thin Solid Films **520**(14), 4792–4796 (2012). https://doi.org/10.1016/j.tsf.2011.10.140
176. L. Wang, J. Li, Y. Wang, K. Yu, X. Tang, Y. Zhang, S. Wang, C. Wei, Construction of 1D SnO_2-coated ZnO nanowire heterojunction for their improved n-butylamine sensing performances. Sci. Rep. **6**(1), 1–12 (2016). https://doi.org/10.1038/srep35079
177. M. Tonezzer, J.H. Kim, J.H. Lee, S. Iannotta, S.S. Kim, Predictive gas sensor based on thermal fingerprints from Pt-SnO_2 nanowires. Sens. Actuators B Chem. **281**, 670–678 (2019). https://doi.org/10.1016/j.snb.2018.10.102
178. T. Li, W. Zeng, Z. Wang, Quasi-one-dimensional metal-oxide-based heterostructural gas-sensing materials: a review. Sens. Actuators B Chem. **221**, 1570–1585 (2015). https://doi.org/10.1016/j.snb.2015.08.003
179. Y. Chen, Y. Cao, Ultrasensitive and low detection limit of acetone gas sensor based on ZnO/SnO_2 thick films. RSC Adv. **10**(59), 35958–35965 (2020). https://doi.org/10.1039/D0RA06406H
180. M. Poloju, N. Jayababu, M.R. Reddy, Improved gas sensing performance of Al doped ZnO/CuO nanocomposite based ammonia gas sensor. Mater. Sci. Eng: B **227**, 61–67 (2018). https://doi.org/10.1016/j.mseb.2017.10.012
181. Z.U. Abideen, J.H. Kim, J.H. Lee, J.Y. Kim, A. Mirzaei, H.W. Kim, S.S. Kim, Electrospun metal oxide composite nanofibers gas sensors: a review. J. Korean Ceram. Soc. **54**(5), 366–379 (2017). https://doi.org/10.4191/kcers.2017.54.5.12
182. Y. Hamedani, P. Macha, T.J. Bunning, R.R. Naik, M.C. Vasudev, *Plasma-Enhanced Chemical Vapor Deposition: Where we are and the Outlook for the Future* (InTech, Vienna, 2016), pp. 247–280
183. D. Tonelli, E. Scavetta, I.I. Gualand, Electrochemical deposition of nanomaterials for electrochemical sensing. Sensors **19**(5), 1186 (2019). https://doi.org/10.3390/s19051186
184. D. Tyagi, H. Wang, W. Huang, L. Hu, Y. Tang, Z. Guo, Y. Tang, Z. Guo, H. Zhang, Recent advances in two-dimensional-material-based sensing technology toward health and environmental monitoring applications. Nanoscale **12**(6), 3535–3559 (2010). https://doi.org/10.1039/C9NR10178K
185. D. Nunes, A. Pimentel, A. Gonçalves, S. Pereira, R. Branquinho, P. Barquinha, E. Fortunato, R. Martins, Metal oxide nanostructures for sensor applications. Semicond. Sci. Technol. **34**(4), 043001 (2019). https://doi.org/10.1088/1361-6641/ab011e
186. Y. Jian, W. Hu, Z. Zhao, P. Cheng, H. Haick, M. Yao, W. Wu, Gas sensors based on chemi-resistive hybrid functional nanomaterials. Nano-Micro Lett. **12**(1), 1–43 (2020). https://doi.org/10.1007/s40820-020-0407-5
187. N.H. Hanh, L. Van Duy, C.M. Hung, N. Van Duy, Y.W. Heo, N. Van Hieu, N.D. Hoa, VOC gas sensor based on hollow cubic assembled nanocrystal Zn_2SnO_4 for breath analysis. Sens. Actuators A Phys. **302**, 111834 (2020). https://doi.org/10.1016/j.sna.2020.111834
188. M.V. Nikolic, V. Milovanovic, Z.Z. Vasiljevic, Z. Stamenkovic, Semiconductor gas sensors: materials, technology, design, and application. Sensors **20**(22), 6694 (2020). https://doi.org/10.3390/s20226694
189. D. Kwak, Y. Lei, R. Maric, Ammonia gas sensors: a comprehensive review. Talanta **204**, 713–730 (2019). https://doi.org/10.1016/j.talanta.2019.06.034
190. J. Dai, O. Ogbeide, N. Macadam, Q. Sun, W. Yu, Y. Li, B.L. Su, T. Hasan, W. Huang, Printed gas sensors. Chem. Soc. Rev. **49**(6), 1756–1789 (2020). https://doi.org/10.1039/C9CS00459A
191. G. Patel, V. Pillai, P. Bhatt, S. Mohammad, Application of nanosensors in the food industry, in *Nanosensors for Smart Cities*. ed. by B. Han, V.K. Tomer, T.A. Nguyen, A. Farmani, P.K. Singh (Elsevier, Amsterdam, 2020), pp. 355–368
192. G. Patel, V. Pillai, M. Vora, Liquid phase exfoliation of two-dimensional materials for sensors and photocatalysis: a review. J. Nanosci. Nanotechnol. **19**(8), 5054–5073 (2019). https://doi.org/10.1166/jnn.2019.16933
193. L. Zhu, W. Zeng, Room-temperature gas sensing of ZnO-based gas sensor: a review. Sens. Actuators Phys. **267**, 242–261 (2017). https://doi.org/10.1016/j.sna.2017.10.02
194. V.S. Bhati, M. Hojamberdiev, M. Kumar, Enhanced sensing performance of ZnO nanostructures-based gas sensors: a review. Energy Rep. **6**, 46–62 (2020). https://doi.org/10.1016/j.egyr.2019.08.070
195. L. Sui, T. Yu, D. Zhao, X. Cheng, X. Zhang, P. Wang, Y. Xu, S. Gao, H. Zhao, Y. Gao, L. Huo, In situ deposited hierarchical CuO/NiO nanowall arrays film sensor with enhanced gas sensing performance to H_2S. J. Hazard. Mater. **385**, 121570 (2020). https://doi.org/10.1016/j.jhazmat.2019.121570
196. P.H. Phuoc, C.M. Hung, N. Van Toan, N. Van Duy, N.D. Hoa, N. Van Hieu, One-step fabrication of SnO_2 porous nanofiber gas sensors for sub-ppm H_2S detection. Sens. Actuators A Phys. **303**, 111722 (2020). https://doi.org/10.1016/j.sna.2019.111722
197. P. Patnaik, *Comprehensive Guide to the Hazardous Properties of Chemical Substances*, 3rd edn. (Wiley, New Jersey, 2007), p. 15
198. Z. Zhu, R.J. Wu, The degradation of formaldehyde using a Pt@TiO_2 nanoparticles in presence of visible light irradiation at room temperature. J. Taiwan Inst. Chem. Eng. **50**, 276–281 (2015). https://doi.org/10.1016/j.jtice.2014.12.022
199. I. Castro-Hurtado, G.G. Mandayo, E. Castaño, Conductometric formaldehyde gas sensors. A review: from conventional films to nanostructured materials. Thin Solid Films **548**, 665–676 (2013). https://doi.org/10.1016/j.tsf.2013.04.083
200. R. Ab Kadir, R.A. Rani, A.S. Zoolfakar, J.Z. Ou, M. Shafiei, W. Wlodarski, K. Kalantar-zadeh, Nb_2O_5 Schottky based ethanol vapour sensors: effect of metallic catalysts. Sens. Actuators B Chem. **202**, 74–82 (2014). https://doi.org/10.1016/j.snb.2014.04.083
201. S.W. Lee, W. Lee, Y. Hong, G. Lee, D.S. Yoon, Recent advances in carbon material-based NO_2 gas sensors. Sens. Actuators B Chem. **255**, 1788–1804 (2018). https://doi.org/10.1016/j.snb.2017.08.203
202. D. Schwela, Air pollution and health in urban areas. Rev. Environ. Health **15**(1–2), 13–42 (2000). https://doi.org/10.1515/REVEH.2000.15.1-2.13
203. F.E. Annanouch, Z. Haddi, S. Vallejos, P. Umek, P. Guttmann, C. Bittencourt, E. Llobet, Aerosol-assisted CVD-grown WO_3 nanoneedles decorated with copper oxide nanoparticles for the selective and humidity-resilient detection of H_2S. ACS Appl. Mater. Interfaces **7**(12), 6842–6851 (2015). https://doi.org/10.1021/acsami.5b00411
204. K. Tian, X.X. Wang, Z.Y. Yu, H.Y. Li, X. Guo, Hierarchical and hollow Fe_2O_3 nanoboxes derived from metal–organic frameworks with excellent sensitivity to H_2S. ACS Appl. Mater. Interfaces **9**(35), 29669–29676 (2017). https://doi.org/10.1021/acsami.7b07069
205. M. Yang, X. Zhang, X. Cheng, Y. Xu, S. Gao, H. Zhao, L. Huo, Hierarchical NiO cube/nitrogen-doped reduced graphene oxide composite with enhanced H_2S sensing properties at low temperature. ACS Appl. Mater. Interfaces **9**(31), 26293–26303 (2017). https://doi.org/10.1021/acsami.7b04969

206. B. Timmer, W. Olthuis, A. Van Den Berg, Ammonia sensors and their applications: a review. Sens. Actuators B Chem. **107**(2), 666–677 (2005). https://doi.org/10.1016/j.snb.2004.11.054
207. The National Institute for Occupational Safety and Health (NIOSH), Preventing carbon monoxide poisoning from small gasoline-powered engines and tools, http://www.cdc.gov/niosh/docs/96-118/default.html. Accessed 08 Oct 2021
208. M. Hjiri, L. El Mir, S.G. Leonardi, A. Pistone, L. Mavilia, G. Neri, Al-doped ZnO for highly sensitive CO gas sensors. Sens. Actuators B Chem. **196**, 413–420 (2014). https://doi.org/10.1016/j.snb.2014.01.068
209. Z. Wang, Z. Li, T. Jiang, X. Xu, C. Wang, Ultrasensitive hydrogen sensor based on Pd0-loaded SnO_2 electrospun nanofibers at room temperature. ACS Appl. Mater. Interfaces **5**(6), 2013–2021 (2013). https://doi.org/10.1021/am3028553
210. R.R. Khan, M.J. Siddiqui, Review on effects of particulates: sulfur dioxide and nitrogen dioxide on human health. Int. Res. J. Environ. Sci. **3**(4), 70–73 (2014)
211. J. Brunet, L. Spinelle, A. Pauly, M. Dubois, K. Guerin, M. Bouvet, C. Varenne, B. Lauron, A. Hamwi, All-organic device with integrated chemical filter dedicated to the selective measurement of NO_2 in air. Org. Electron. **11**(7), 1223–1229 (2010). https://doi.org/10.1016/j.orgel.2010.04.021
212. Z. Li, Y. Liu, D. Guo, J. Guo, Y. Su, Room-temperature synthesis of CuO/reduced graphene oxide nanohybrids for high-performance NO_2 gas sensor. Sens. Actuators B Chem. **271**, 306–310 (2018). https://doi.org/10.1016/j.snb.2018.05.097
213. D. Van Sickle, M.A. Wenck, A. Belflower, D. Drociuk, J. Ferdinands, F. Holguin, E. Svendsen, L. Bretous, S. Jankelevich, J.J. Gibson, R.L. Moolenaar, Acute health effects after exposure to chlorine gas released after a train derailment. Am. J. Emerg. Med. **27**(1), 1–7 (2009). https://doi.org/10.1016/j.ajem.2007.12.006
214. C. Winder, The toxicology of chlorine. Environ. Res. **85**(2), 105–114 (2001). https://doi.org/10.1006/enrs.2000.4110
215. C.W. White, J.G. Martin, Chlorine gas inhalation: human clinical evidence of toxicity and experience in animal models. Proc. Am. Thorac. Soc. **7**(4), 257–263 (2010). https://doi.org/10.1513/pats.201001-008SM
216. T. Miyata, T. Hikosaka, T. Minami, High sensitivity chlorine gas sensors using multicomponent transparent conducting oxide thin films. Sens. Actuators B Chem. **69**(1–2), 16–21 (2000). https://doi.org/10.1016/S0925-4005(00)00301-4
217. J. Tamaki, C. Naruo, Y. Yamamoto, M. Matsuoka, Sensing properties to dilute chlorine gas of indium oxide based thin film sensors prepared by electron beam evaporation. Sens. Actuators B Chem. **83**(1–3), 190–194 (2002). https://doi.org/10.1016/S0925-4005(01)01039-5
218. P. Van Tong, N.D. Hoa, N. Van Duy, N. Van Hieu, Micro-wheels composed of self-assembled tungsten oxide nanorods for highly sensitive detection of low level toxic chlorine gas. RSC Adv. **5**(32), 25204–25207 (2015). https://doi.org/10.1039/C5RA00916B
219. A. Singh, Z. Salmi, N. Joshi, P. Jha, P. Decorse, H. Lecoq, S. Lau-Truong, M. Jouini, D.K. Aswal, M.M. Chehimi, Electrochemical investigation of free-standing polypyrrole–silver nanocomposite films: a substrate free electrode material for supercapacitors. RSC Adv. **3**(46), 24567–24575 (2013). https://doi.org/10.1039/C3RA42786B
220. A. Singh, Z. Salmi, P. Jha, N. Joshi, A. Kumar, P. Decorse, H. Lecoq, S. Lau-Truong, D.K. Aswal, D.S.K. Gupta, M.M. Chehimi, One step synthesis of highly ordered free standing flexible polypyrrole-silver nanocomposite films at air–water interface by photopolymerization. RSC Adv. **3**(32), 13329–13336 (2013). https://doi.org/10.1039/C3RA40884A
221. A. Singh, Z. Salmi, N. Joshi, P. Jha, A. Kumar, H. Lecoq, S. Lau, M.M. Chehimi, D.K. Aswal, S.K. Gupta, Photo-induced synthesis of polypyrrole-silver nanocomposite films on N-(3-trimethoxysilylpropyl) pyrrole-modified biaxially oriented polyethylene terephthalate flexible substrates. RSC Adv. **3**(16), 5506–5523 (2013). https://doi.org/10.1039/C3RA22981E
222. N. Joshi, V. Saxena, A. Singh, S.P. Koiry, A.K. Debnath, M.M. Chehimi, D.K. Aswal, S.K. Gupta, Flexible H_2S sensor based on gold modified polycarbazole films. Sens. Actuators B Chem. **200**, 227–234 (2014). https://doi.org/10.1016/j.snb.2014.04.041
223. E.P. Stuckert, E.R. Fisher, Ar/O_2 and H_2O plasma surface modification of SnO_2 nanomaterials to increase surface oxidation. Sens. Actuators B Chem. **208**, 379–388 (2015). https://doi.org/10.1016/j.snb.2014.11.049
224. H. Liu, Y. Chu, Y. Liu, T. Hayasaka, Z. Shao, N. Joshi, X. Wang, Z. You, L. Lin, Label-free AC sensing by a graphene transistor for 100-ppb formaldehyde in air. In, *2019 IEEE 32nd International Conference on Micro Electro Mechanical Systems (MEMS)*, pp. 488–491 (2019). https://doi.org/10.1109/MEMSYS.2019.8870717
225. H. Liu, Y. Liu, Y. Chu, T. Hayasaka, N. Joshi, Y. Cui, X. Wang, Z. You, L. Lin, AC phase sensing of graphene FETs for chemical vapors with fast recovery and minimal baseline drift. Sens. Actuators B Chem. **263**, 94–102 (2018). https://doi.org/10.1016/j.snb.2018.01.244
226. H. Liu, Y. Chu, Y. Liu, T. Hayasaka, N. Joshi, Y. Cui, X. Wang, Z. You, L. Lin, Selective sensing of chemical vapors using phase spectra detection on CVD graphene fet. In, *2018 IEEE Micro Electro Mechanical Systems (MEMS)*, pp. 210–213 (2018). https://doi.org/10.1109/MEMSYS.2018.8346521
227. Health Link BC, Indoor air quality: volatile organic compound (VOCs), https://www.healthlinkbc.ca/healthlinkbc-files/air-quality-VOCs. Accessed 08 Oct 2021

Publisher's Note Springer Nature remains neutral with regard to jurisdictional claims in published maps and institutional affiliations.